

Full Length Article

Evaluation of impact of surface diffusion on methane recovery via carbon dioxide injection in shale reservoirs

Dimitris Spanakos, Sean P. Rigby

Department of Chemical and Environmental Engineering, University of Nottingham, University Park, Nottingham NG7 2RD, UK



ARTICLE INFO

Keywords:

Shale gas
CO₂ injection
Reservoir modelling
Surface diffusion
Fractal theory

ABSTRACT

Injection of carbon dioxide into shale reservoirs is a promising technology for enhancing natural gas recovery and reducing greenhouse gas emissions. Nanoscale phenomena contribute to a significant difference in mass transfer processes within shale-gas reservoirs compared to conventional gas reservoirs. Previous investigations have shown the significance of surface diffusion to gas transfer mechanisms. Surface diffusion was added to an established apparent permeability model, which was then applied for the first time to numerical reservoir simulations to model CO₂ injection techniques. Most publications to date have used a theoretical model to predict surface diffusion coefficient in a low-pressure condition, whereas, in this paper, it has been estimated from gravimetric experiments. Shale reservoirs, with different reservoir and petrophysical properties, were generated to investigate the efficiency of transport of CO₂ via surface diffusion. A recently proposed fractal model for surface diffusion was used to investigate the impact of rock surface roughness on CH₄ production. The results show that surface diffusion plays a significant role in increasing CH₄ recovery by up to 3.2% when the average pore radius is less than 2 nm. In particular, a high surface fractal dimension can potentially enhance CH₄ production by up to 1.5% and should not be neglected when the average pore radius is less than 1 nm. In areas with high surface capacity, adsorption of CO₂ and desorption of CH₄ molecules may increase by up to 2.74% and 2.3%, respectively, when compared to models with no surface diffusion. In all the reservoirs examined, geo-statistical reservoir simulations showed that reservoir heterogeneity is not favourable to methane recovery via CO₂ injection techniques, except for the Barnett shale reservoir. To the best of our knowledge, this work is the first to implement an apparent model within a reservoir simulator to investigate the impact of surface diffusion on methane recovery via CO₂ injection techniques at various shale reservoirs with different properties.

1. Introduction

The world today is faced with a scarcity of conventional energy sources due to population growth and technological advancement [1,2]. The global demand of natural gas is predicted to increase by 45% by 2040, and 30–50% of its supply is expected to come from shale gas [3]. The production potential of shale gas reservoirs, which are amenable to hydraulic fracturing and horizontal drilling techniques, has been scrutinized in order to overcome the depletion of conventional reservoirs and to supply the world with greater quantities of clean-burning energy [4]. As a result, there has been a paradigm shift in thinking towards unconventional gas that is now, to a large extent, changing the world energy landscape, leading to a rapid expansion of shale gas production, especially over the past decade. In particular, there has been an increase in supply from the shale resources in North America [5]. For example, the Marcellus Shale is situated in the Appalachian basin, where it has a

total area of greater than 100,000 miles, and its depth ranges between 4000 and 8500 ft, having an average thickness of 50–200 ft. [6]. The Marcellus Shale has been estimated to contain 1500 TCF (trillion cubic feet) of original gas in place (OGIP) and has 141 TCF of technically recoverable gas [6]. CO₂ injection is also used for enhanced oil recovery [7].

In a normal production process for shale gas, the free gas in large pores and fractures usually comes out first and its production usually lasts for just under two years [8]. In the later production processes, the dominant source of gas is then adsorbed gas because the small pores in shale have slow desorption kinetics which restricts diffusion from the matrix [9]. Subsequently, after few years of production from the shale gas well, the gas rate declines steeply. Thus, there has been a growing interest in enhanced shale gas recovery (ESGR) via carbon dioxide (CO₂) injection.

Even though rare field tests are reported for the CO₂-ESGR injection

E-mail address: Dimitris.Spanakos@nottingham.ac.uk (D. Spanakos).

<https://doi.org/10.1016/j.fuel.2021.121928>

Received 24 March 2021; Received in revised form 27 July 2021; Accepted 4 September 2021

Available online 11 September 2021

0016-2361/© 2021 The Authors. Published by Elsevier Ltd. This is an open access article under the CC BY license (<http://creativecommons.org/licenses/by/4.0/>).

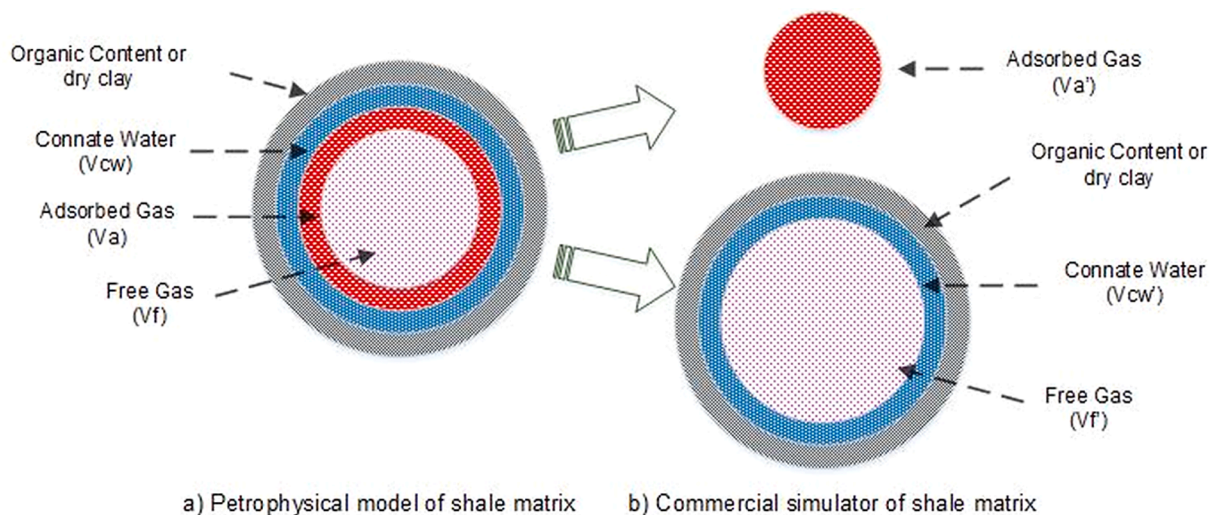


Fig. 1. Schematic diagram illustrating the volume fractions of shale matrix in a) Wang et al. [26] petrophysical model and b) commercial reservoir simulator.

technique [10,11], there are both experimental and numerical studies conducted to assess its suitability in the exploration and production of shale [12–16]. According to a number of studies, CO_2 sorption affinity to the shale is greater than that of CH_4 in the subsurface situation [17,18]. In shale gas reservoirs, CO_2 injection does not just improve the production of CH_4 but also enables CO_2 sequestration.

In general, shales can be the seal, the reservoir, and/or the hydrocarbon source. Typically, the properties of gas shale include a very low permeability, of the order of nano-Darcy (10^{-6} mD), a very small grain size, increased total organic carbon (TOC), and a small porosity. Gas hold-ups in shale reservoirs are mainly made up of bulk gas within the pore space and gas adsorbed on the internal shale matrix [19–21]. According to past studies, gases are adsorbed in the nanopores of clay minerals and organic matter, which make up the larger part of shale [22–24]. Notably, adsorbed gas is estimated to be up to 20%–80% of the total gas in place (OGIP) in five of United States shale formations, while a study conducted by Lu et al. [25] for 24 Devonian shales found that adsorbed gas can average 61% of the total gas volume. A study conducted by Wang et al. [26] showed that, without the appropriate petrophysical corrections to commercial simulators (Eclipse, CMG, VIP) when considering gas adsorption, the original gas in place (OGIP) can be overestimated by approximately 50%.

In addition, shale-gas reservoirs (SGRs) have a gas mass-transfer process exhibiting a significant rate difference from that seen in conventional gas reservoirs. This kind of variation is ultimately attributed to the presence of organic matter and particular nano-scale phenomena. According to Xiong et al. [27] and Firouzi et al. [28] the diameter of organic pores is usually below 10 nm and accounts for 42% of the total volume. Moreover, the diameter of nanopores is comparable to the order of the gas molecular mean free path at reservoir conditions. The gas transfer regimes, occurring within the SGRs, include both bulk gas transfer and surface diffusion mechanisms. The latter regime tends to have been overlooked by previous researchers, who have conducted reservoir simulations [29,30] to investigate the practical feasibility of use of CO_2 for gas extraction from shale reservoirs. Subsequently, gas production predicted may be significantly overestimated or underestimated. Further, researchers have shown the importance of Knudsen diffusion to the pore transport mechanism in nanopores and a study conducted by Darabi et al. [31] showed that Knudsen diffusion contributes around 20% of the total produced gas at typical SGR conditions. Experimental studies have also been made of transport and phase changes in fabricated nanofluidic models for shale rocks [31,32]. However, while these model pore networks studied have included pore body-pore neck geometries, they are only 2D planar and thus miss the

full three-dimensional connectivity of real rocks. These models also have only limited spatial extent and thus miss the impact of longer-range heterogeneities. Further, these experiments also only considered transport by Knudsen diffusion and viscous flow.

However, other experimental investigations have also indicated that, in comparison to bulk gas transport, surface diffusion, is more significant where the pore network is not yet well-evolved within shale gas reservoirs [33,34]. This means that, surface diffusion dominates in the microporous kerogen due to high surface area and the non-development of fractures within shales. It has also been shown that the surface diffusion of adsorbed gas and the Knudsen diffusion of the free gas, can increase the apparent permeability of the SGRs. Previous studies have indicated that the estimated apparent permeability may be several orders of magnitude higher than that of conventional hydrodynamic techniques (i.e. the Darcy and Klinkenberg models) [31,36,37]. Hence, it is reasonable to say that the surface diffusion of adsorbed gas and the Knudsen diffusion of the free gas, can increase the apparent permeability of the SGRs and must be included to ensure accurate prediction of gas recovery, despite them generally being omitted in previous work.

In this paper, a new dual permeability-dual porosity model of the Marcellus shale reservoir will be primarily generated based on existing geological data. The Langmuir isotherm is considered as a model for adsorption in different areas of Marcellus shale. Then, the bulk porosity, free gas saturation, and connate water saturation of the models are corrected, *a priori*, according to Wang's theory [38] to avoid over-estimation of the volume of free gas and the original gas in place. Fracture height, fracture half-length, and fracture conductivity were the main fitting parameters used to obtain a good history match with gas field data [29]. Thereafter, surface diffusion is implemented into a reservoir scale simulator. This was achieved by utilizing an established approach based on apparent permeability model that included surface diffusion [39]. Most publications to date have used a theoretical model to predict surface diffusivity in a low-pressure condition [40,41]. In this study, the adsorbed-gas surface diffusivity in a low-pressure condition is estimated from gravimetric gas uptake experiments on Marcellus shale samples. In addition, Barnett and New Albany reservoir models are also generated from previous studies to investigate the significance of surface diffusion to CO_2 injection techniques in these locales. A recently proposed fractal theory for surface diffusivity [42] is applied, for the first time, to all reservoir models to permit the examination of the effects of degree of surface roughness on CH_4 production and CO_2 adsorption. Finally, a geostatistical approach is applied to assess the effect of larger-scale reservoir heterogeneity on gas production. The goal of this paper is to provide insights into a better understanding of the effectiveness of

surface diffusion on methane recovery via CO₂ injection techniques at shale reservoir scale.

2. Theory

2.1. Multicomponent adsorption

According to previous studies, adsorbed methane could be responsible for 5–30% of the entire gas production in shale gas reservoirs [43–45]. Adsorption trapping is also a dominant means for storing CO₂, because the adsorption interaction of CO₂ with a highly organic shale is five times stronger than that of CH₄ [11]. To formulate a model that includes competitive multi-component adsorption/desorption, the extended Langmuir isotherm has been identified as providing a good description of the binary gas sorption of CO₂ and CH₄, and, thus is applied in the current study. The generalised multi-component Langmuir isotherm is given as [46,47]:

$$\alpha_{\zeta} = \frac{\alpha_{\zeta\max} b_i \gamma_{\zeta g} P}{1 + P \sum_{\zeta} b_j \gamma_{\zeta g}} \quad (1)$$

where α_{ζ} represents the quantity of adsorbed component ζ in moles per unit rock mass, $\alpha_{\zeta\max}$ represents the highest quantity of adsorbed component ζ in moles for each unit mass of rock, b_i represents the energy of interaction parameter for the Langmuir isotherm relation, $\gamma_{\zeta g}$ represents the molar fraction of adsorbed component i in the gas phase, and P represents the pressure. $\alpha_{\zeta\max}$ and b_i depend upon the total organic content (TOC) of the shale and must be measured experimentally for core samples.

Wang et al. [26] demonstrated a feasible approach to correct the petrophysical properties of shale gas reservoirs effectively within commercial reservoir simulators when considering gas adsorption. Fig. 1 is a schematic depiction of the volumetric constituents of the nanopores within a typical shale matrix in both the petro-physical model and a commercial reservoir simulator. In commercial simulators, the volume of adsorbed gas is frequently treated as polymer, alkali or other chemical agents, or is often ignored. However, adsorbed gas comprises 20%–80% of the total gas in place and should not be overlooked as discussed in section 1.

As illustrated in Fig. 1b, the total void volume (V_t') is equal to the sum of the connate water volume (V_{cw}') and the free gas volume (V_f'). In contrast, the total void volume (V_t) in the petrophysical model is equal to the sum of the connate water (V_{cw}), free gas (V_f), and gas adsorbed (V_a) (Fig. 1a). Hence, the total void volumes (V_t') and porosity (ϕ_t') of both the petrophysical model and commercial simulator are expressed as:

$$V_t' = V_{cw}' + V_f' < V_t = V_{cw} + V_f + V_a \quad (2)$$

$$\phi_t' = \phi_{cw}' + \phi_f' = \phi_{cw} + \phi_f = \phi_t - \phi_a \quad (3)$$

where ϕ_{cw} and ϕ_a are the connate water porosity and adsorbed gas porosity, respectively. Eqs. (2) and (3) show that the free gas volume and porosity in the commercial simulator are overestimated, and, thus both the total void volume and porosity in the simulator should be less than that in Wang's petrophysical model of the shale matrix. Subsequently, bulk porosity, free gas saturation, and connate water saturation were corrected in order to accurately predict the gas production and reduce the error of OGIP. The theory behind the derivations will be given only briefly, since it is described extensively in previous paper [26].

Ambrose [48] proposed a new method for obtaining the storage capacities of both adsorbed and free gas. The storage capacities of free gas (G_f) and adsorbed gas (G_a) on the basis of Langmuir isotherm are:

$$G_a = V_L \left(\frac{P/Z}{P/Z + P_L} \right) \quad (4)$$

$$G_f = \frac{32.0368}{B_{gf}} \left[\frac{\phi_t(1 - S_w)}{\rho_r} - \frac{1.318 \times 10^{-6} M}{\rho_{ga}} G_a \right] \quad (5)$$

where B_{gf} is the free gas volume factor, P_L is the Langmuir pressure, V_L is the Langmuir volume, S_w is the water saturation, ρ_r is the rock density, ρ_{ga} the adsorbed gas density and Z is the gas factor. Moreover, Ambrose et al. [48] showed that the density of free gas and adsorbed gas is different in the shale matrix nanopore. Hence, the porosity ratio of free gas and adsorbed gas in the petrophysical model is:

$$\frac{\phi_{gf}}{\phi_{ga}} = \frac{V_{gf}}{V_{ga}} = \frac{G_f \cdot \rho_{ga}}{G_a \cdot \rho_{gf}} \quad (6)$$

Hence,

$$\phi_{ga} = \frac{\phi_{gf} \cdot G_a \cdot \rho_{gf}}{G_f \cdot \rho_{ga}} \quad (7)$$

At connate saturation, the total gas porosity is:

$$\phi_{gf} + \phi_{ga} = \phi_t(1 - S_{wc}) \quad (8)$$

Substituting Eqs. (2) and (7) into Eq. (8), the corrected bulk porosity in the commercial simulator is:

$$\phi_t' = \phi_{gf} + \phi_{cw} = \phi_t - \frac{\phi_{gf} \cdot G_a \cdot \rho_{gf}}{G_f \cdot \rho_{ga}} \quad (9)$$

The connate water saturation and free gas saturation in the simulation model are:

$$S_{wc}' = \frac{\phi_t \cdot S_{wc}}{\phi_t'} = \frac{G_f \cdot \rho_{ga} \cdot \phi_t \cdot S_{wc}}{G_f \cdot \rho_{ga} \cdot \phi_t - \phi_{gf} \cdot G_a \cdot \rho_{gf}} \quad (10)$$

$$S_{gf}' = \frac{G_f \cdot \rho_{ga} \cdot \phi_t' \cdot (1 - S_{wc}') - \phi_{gf} \cdot G_a \cdot \rho_{gf}}{G_f \cdot \rho_{ga} \cdot \phi_t' - \phi_{gf} \cdot G_a \cdot \rho_{gf}} \quad (11)$$

Consequently, the total porosity, water saturation and gas saturation used in the commercial reservoir simulator are calculated, *a priori*, according to Eqs. (9)–(11) respectively. It should be mentioned that these equations have already been validated in previous studies using field data obtained from Marcellus and Barnett shale [26,38].

2.2. Multiple flow mechanisms for shale gas

Numerical simulations play a major role in comprehending and forecasting the production of gas and oil from reservoirs. In industry a range of commercial reservoir simulator packages are used. However, mass transport within reservoir models constructed with these commercial simulators is generally based upon Darcy's law, and, thence neglects certain gas transfer mechanisms that exist within the SGRs. As a result, the shale gas production forecasted can be overestimated, or underestimated, when the apparent permeability, which is the transport parameter that includes provision for these additional mechanisms, is not used. Previous studies have demonstrated [38,39] that the Darcy flow permeability can be corrected for additional transport mechanisms via multipliers, which are functions of gas pressure and are input into the simulator model.

The theory behind the derivation of the apparent permeability approach will only be given briefly here, since it is described in more detail in other work [39,49,50]. The mass flux for total fluid transfer, J_b , is given by:

$$J_t = J_b + J_s = \frac{1}{1 + Kn} \cdot \omega_s \cdot \omega_m \cdot J_{vs} + \frac{1}{1 + 1/Kn} \cdot \omega_s \cdot \omega_m \cdot J_k + J_s \quad (12)$$

where J_b is the mass flux of the bulk gas transfer and J_s is the mass flux of the adsorbed gas surface diffusion. J_b includes the contributions from J_{vs} and J_k , which are the slip-flow flux and Knudsen diffusion flux, respectively. ω_m and ω_s are the poromechanical, and the sorption-

induced, swelling response coefficients of the shale matrix, respectively. From eq.12, it can be observed that the adsorbed-gas flux and bulk-gas flux are determined from a simple sum, whereas the resultant gas flux in the bulk transfer phase is obtained by taking the weighted sum of Knudsen diffusion flux and slip-flow flux based on their respective contributions. Moreover, eq. (12) demonstrates a correlation, for both the poromechanical and sorption-induced swelling responses, to the bulk gas flux, which varies with permeability during the development of SGRs [51].

2.2.1. Continuum flow of free gas

Continuum no-slip flow, or Darcy flow, occurs when the Knudsen number (Kn) $< 10^{-3}$. The collisions between molecules then dominate, and, thus the gas flow is continuum flow, which can be expressed according to the Hagen–Poiseuille equation [52]:

$$J_v = -\zeta_{mb} \frac{r^2 P}{8\mu RT} \frac{dp}{dl} \quad (13)$$

where

$$\zeta_{mb} = \frac{\varepsilon}{\tau} \quad (14)$$

where J_v is the continuum-flow, ζ_{mb} is a dimensionless correction factor of apparent permeability, μ is the gas viscosity, P is the pressure, R is the universal gas constant, l is the gas transport distance, T is the temperature, ε is the porosity, τ is the tortuosity (equal to 1.8) [42], and r is the nanopores radius.

2.2.2. Slip flow of free gas

Slip flow occurs when $10^{-3} < Kn < 10^{-1}$, where gas molecules slip on the nanopore wall. In addition, both the intermolecular collisions, and collisions between gas molecules and nanopore walls, are similarly dominant. The slip boundary condition was achieved by modifying the no-slip boundary condition in continuum flow [53]:

$$J_{vs} = -\frac{1}{1+Kn} \zeta_{mb} \omega_s \omega_m \frac{r^2 P}{8\mu RT} (1 + \alpha Kn) \left(1 + \frac{4Kn}{1 - \psi Kn} \right) \frac{dP}{dl} \quad (15)$$

where ψ is the dimensionless gas-slip constant and α the dimensionless rarefaction coefficient.

2.2.3. Knudsen diffusion of free gas

Knudsen diffusion arises for $Kn \geq 1$, when collisions between gas molecules and nanopore walls dominate. Assuming that the pore is circular in cross-section, with a radius r , and taking into account the wall roughness, the Knudsen equation can be expressed as [35,52]:

$$J_k = -\frac{1}{1+1/Kn} \frac{2}{3} \zeta_{mb} \omega_s \omega_m r \delta^{D_f-2} \left(\frac{8}{\pi RTM} \right)^{0.5} \frac{dP}{dl} \quad (16)$$

where

$$D_k = \frac{2}{3} \zeta_{mb} \left(\frac{8RT}{\pi M} \right)^{0.5} \quad (17)$$

where D_k is the Knudsen diffusion coefficient, δ the ratio of the gas molecule diameter, D_f the fractal dimension of the pore wall and M the gas molar mass.

2.3. Surface diffusion of adsorbed gas

Surface diffusion plays a significant role in mass transport within the nanopores of shale, wherein there is organic matter with a large surface area, and, thence, in the overall gas mass transfer [12,27,54,55]. During gas phase mass transfer in nanopores, the surface diffusion of adsorbed gas is characterised by a large concentration gradient, which plays a

crucial role in this process [35]. Surface diffusion is a physical process that entails a random hopping mechanism, such that the adsorbed particles periodically escape from, and move between, lower-energy adsorption sites. The activated molecules can, thence, jump between fixed sites with a specific velocity, which leads to surface migration in the adsorbed phase. Once a molecule acquires enough energy to fully escape from the surface, it returns to the gaseous state.

Previous studies have shown that it is more appropriate to investigate shale gas sorption by using the Langmuir isotherm which is based on single-layer adsorption [56,57]. Thus, the hopping model can be most appropriate to surface diffusion of adsorbed gas in shales. Various researchers established different classical hopping models. For instance, a widely used analytical mode was developed by Hwang and Kammermeyer [40] and Guo et al. [41] for low-pressure conditions where the equation of the surface diffusion coefficient is influenced by temperature, adsorbent and adsorbate. However, this model overpredicts surface diffusivity at low pressure, which is an observation made by Do [58]. In particular, Do [58] estimated surface diffusivities by analyzing kinetic data collected using three different kinetics methods: constant molar flow, the differential adsorption bed, and the differential permeation methods. The experimental results showed that the apparent surface diffusivity decreases very rapidly with molecular weight, and much more strongly than the inverse of the square root of molecular weight, as obtained by Hwang and Kammermeyer [40] and Guo et al. [41], and, thus this latter model will not be used. In contrast, the surface diffusivity at zero coverage was obtained using a dual-diffusion model [59] and the analysis will be given in Section 2.3.1.

In order to simplify the treatment of the contribution of surface diffusion to flow in the reservoir simulations, the component of effective permeability resulting from surface diffusion will be estimated using the properties of carbon dioxide alone. This assumption means that the impact of surface diffusion on methane production estimated below is likely to be a lower limit, given the relatively higher mobility of methane compared with carbon dioxide. In order to estimate the contribution of surface diffusion to effective permeability a series of models were used. First, an estimate of the surface diffusivity at zero coverage on a reference shale was obtained using a dual-diffusion model to analyse low pressure gas uptake experiments. Second, if considering simulations in shales other than the reference, this zero-coverage surface diffusivity was adjusted for the influence of different surface roughness between shales using a fractal model. Third, where the pressure was such that the surface coverage was above zero the surface diffusivity was also adjusted accordingly using a model for the impact of surface occupancy on migration. The resultant surface diffusivity was then used to obtain the contribution of surface diffusion to the effective permeability for a particular shale.

2.3.1. Surface diffusivity at low pressure

Experimental measurements of kinetic gas uptake into a reference shale material were used to estimate the surface diffusivity of carbon dioxide at the limit of surface coverage tending to zero. The analysis of the experimental kinetic data was performed using the dual-diffusion model proposed by Do and Rice [59]. This analysis was used to obtain an estimate of the surface diffusivity at zero coverage for the reference surface. The Do and Rice model is an approximate analytical solution for the uptake half-time considering particle size, Langmuir constant, maximum adsorption capacity, and pore and surface diffusivity. The model is given by the expressions:

$$\Omega = \varepsilon_M D_p + (1 - \varepsilon_M) D_{so} \Xi \quad (18)$$

where:

$$\Omega = \frac{AR^2 [\varepsilon_M + (1 - \varepsilon_M) \frac{C_{p0}}{C_0}] (1 - \frac{BbC_0}{1 + \gamma b C_0})}{t_{0.5}} \quad (19)$$

and

$$\Xi = \left(1 - \frac{BbC_0}{1 + \Gamma bC_0}\right) \left(\frac{C_{\mu 0}}{C_0}\right) \quad (20)$$

where $C_{\mu 0}$ (mole/volume of solid) is the adsorbed amount in equilibrium with the bulk concentration C_0 (mole/volume of fluid); ε_M is the local porosity; A, B, Γ are the shape factors depending on the shape of the adsorbent particles, and b is the Langmuir constant which can be described using the local Langmuir isotherm:

$$C_{\mu 0} = C_{\mu s} \frac{bC_0}{1 + bC_0} \quad (21)$$

Eq. (18) implies that if one plots Ω versus Ξ , a straight line will be thereby obtained, whose intercept ($\varepsilon_M D_p$) and slope $(1 - \varepsilon_M) D_{so}$ are related to pore and surface diffusivities. Moreover, Eq. (18) is valid for any of the three possible ideal shapes of the solid particle, namely the slab, cylinder and sphere, whose corresponding factors are α, β, γ , respectively. The sample particles used in this work have a roughly spherical shape and will be analysed as such in Section 3. However, the model was applied in a low-pressure condition, and, thus cannot be used for calculating surface diffusion of adsorbed gas in a high-pressure condition.

2.3.2. Fractal theory for surface diffusivity at low pressure

The difference in surface diffusion rates between different shales resulting from variation in surface roughness was determined using a fractal model. Recently, Spanakos and Rigby [42] showed that, for shales, both the pre-exponential factor and the activation energy for surface diffusivity are functions of the surface fractal dimension, and, thus the surface diffusivity on shales could be established from an equilibrium gas adsorption isotherm. Hence, the surface diffusivities for new surfaces can be obtained from measurements performed on a reference material and knowledge of the surface fractal dimension for the new surface. The theory behind the derivations below will be given briefly, since it is described in more detail elsewhere [42,60]. In an activated process of surface diffusion, in which the rate varies with temperature, the surface diffusivity can often be estimated using the Arrhenius expression:

$$D_{so} = D_o \exp\left(\frac{-E_D}{RT}\right) \quad (22)$$

where D_o is the pre-exponential factor and E_D is the activation energy for diffusion.

The pre-exponential factor is the entropic term, and can be given by the expression:

$$\ln D_o = [\ln D_{or} - d_r \ln\left(\frac{R_\infty}{r_s}\right)] + d \ln\left(\frac{R_\infty}{r_s}\right) \quad (23)$$

where d_r is the fractal dimension for a reference material, R_∞ is the apparent limiting upper length scale cutoff for the area within the molecular jump range as the temperature tends to infinity, and r_s the cross-sectional area of the molecule.

The activation energy is the enthalpy term and is given by the expression:

$$E_D = w + x \left(\frac{R_n}{r_s}\right)^d \quad (24)$$

where w and x are terms composed only of constants relating to the strength of the interactions with the surface. R_n represents the distance from the middle of a molecule to the furthest edge of an immediately adjacent site. In this work, where the model is used to predict surface diffusivity at zero coverage, the lateral interactions of the diffusing molecule are envisaged to be with the solid surface in adjacent empty adsorption sites, rather than neighbouring molecules, as for the case of monolayer coverage studied previously. Eqs. (23) and (24) demonstrate that both the pre-exponential factor and the activation energy are linear

functions of the fractal dimension d and the group $(R_n/r)^d$, respectively.

2.3.3. Surface diffusivity at high pressure

The impact, on surface flow of surface occupancies above the zero limit, was obtained using the Chen and Yang model [61]. These authors established a surface diffusion model describing the influence of adsorbed-gas coverage from a hopping model. In particular, a kinetic method was applied to derive the surface diffusion coefficient under a high-pressure condition such that:

$$D_s = D_{so} \frac{(1 - \theta) + \frac{\kappa}{2} \theta (2 - \theta) + [H(1 - \kappa)] (1 - \kappa) \frac{\kappa}{2} \theta^2}{\left(1 - \theta + \frac{\kappa}{2} \theta\right)^2} \quad (25)$$

$$H(1 - \kappa) = \begin{cases} 0, & \kappa \geq 1 \\ 1, & 0 \leq \kappa \leq 1 \end{cases} \quad (26)$$

$$\kappa = \frac{\kappa_b}{\kappa_m} \quad (27)$$

where D_s is the gas surface diffusion coefficient; θ is the dimensionless gas coverage; $H(1 - \kappa)$ is the dimensionless Heaviside function; κ is the ratio constant for blockage to the rate constant for forward migration and takes a value of 0.5 [49]; κ_b and κ_m are the coefficients for surface-gas molecules for the blocking velocity and forward velocity, respectively.

According to Eq. (18), D_{so} is initially estimated via gravimetric experiments using the dual-diffusion model and implemented in Eq. (25). Thereafter, in cases where the surface roughness for shales was other than that of the reference, the fractal model in Eq. (22) was applied to estimate D_{so} .

2.3.4. Surface diffusion contribution to effective permeability

According to previous studies [39,49,50] the apparent permeability of adsorbed gas surface diffusion can be expressed as:

$$k_s = - \frac{J_s V_{std} \mu}{M dP/dx} = \zeta_{ms} D_s \frac{C_s V_{std} \mu}{PM} \quad (28)$$

where

$$\zeta_{ms} = \frac{\phi}{\tau} \left[\left(1 - \frac{d_M}{r}\right)^{-2} - 1 \right] \quad (29)$$

and

$$C_s = \frac{4\theta M}{\pi d_M^3 N_A} \quad (30)$$

$$\theta = \frac{P}{P_L + P} \quad (31)$$

where C_s is the adsorbed gas concentration; ζ_{ms} is the correction factor of surface diffusion of adsorbed gas; d_M is gas molecular diameter; and N_A is Avogadro's constant.

Eq. (28) is based on the combination of the Maxwell-Stefan method, which states that the driving force of surface diffusion is a chemical potential gradient, and the assumption that the gas behaves as an ideal gas [62,63].

2.4. Apparent permeability model flow gas transfer in shale nanopores

The gas transfer mechanisms discussed above include slip flow, Knudsen diffusion, and surface diffusion in the nanopores of SGRs. The sum of each gas flux mechanism comprises the total gas flux. While the adsorbed-gas flux and bulk-gas flux are determined from a simple sum, the slip-flow flux and Knudsen diffusion flux are determined from the weighted sum.

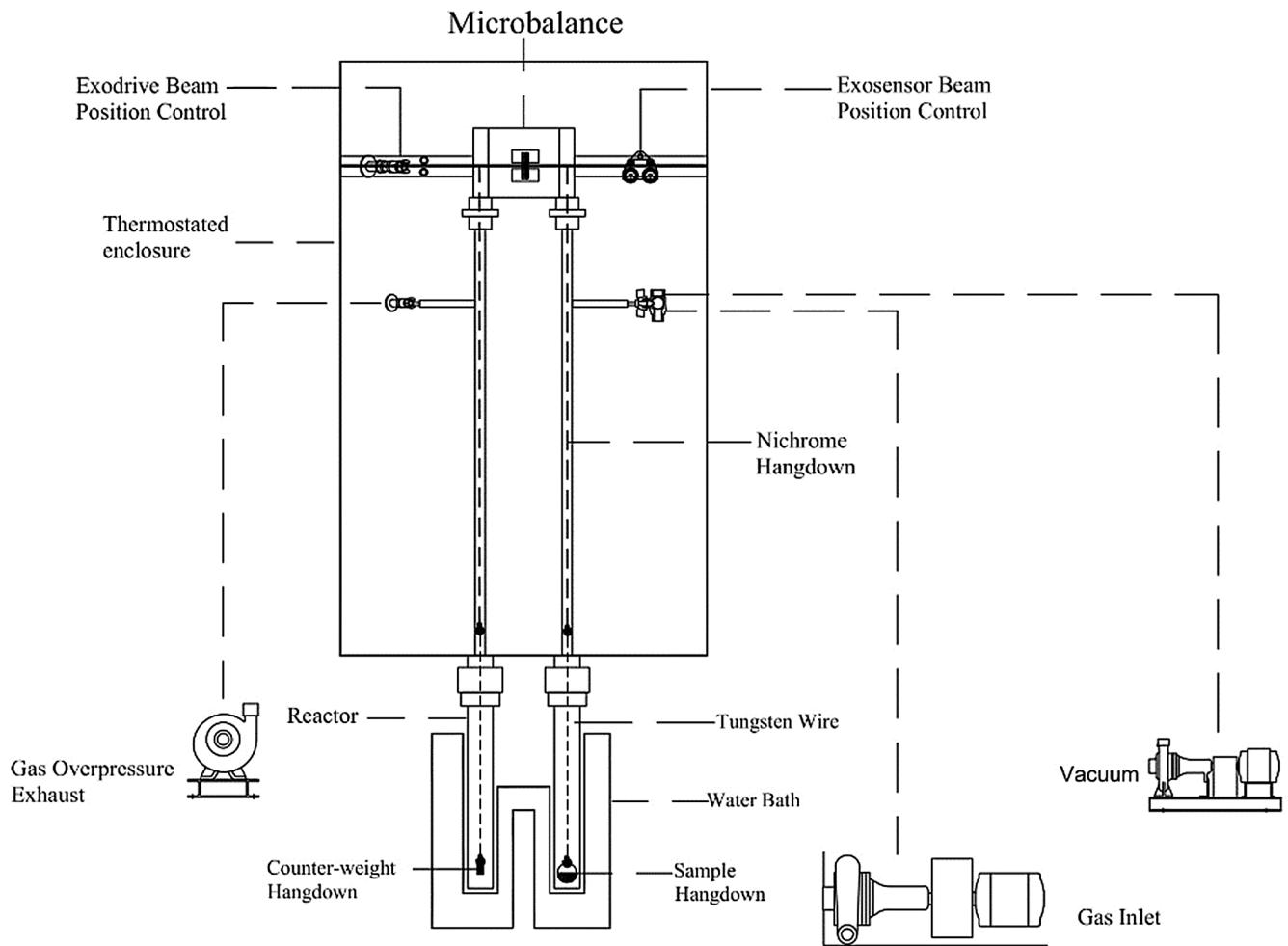


Fig. 2. Schematic diagram of the Xemis gravimetric Analyser (Spanakos and Rigby [42], reproduced under Creative Commons licence CC-BY).

By combining Eqs. (15), (16), and (28), the apparent permeability for the total gas transport through shale nanopores, comprising of slip flow, Knudsen diffusion and surface diffusion, is expressed as:

$$k_t = k_{vs} + k_k + k_s \quad (32)$$

where

$$k_{vs} = \frac{1}{(1 + Kn)} \zeta_{mb} \omega_m \omega_s \frac{r^2 (1 + \alpha Kn)}{8} \left(1 + \frac{4Kn}{1 - \psi Kn} \right) \quad (33)$$

$$k_k = \frac{1}{(1 + 1/Kn)} \zeta_{mb} \omega_m \omega_s \frac{2}{3} r \delta^{D_f - 2} \left(\frac{8RT}{\pi M} \right)^{0.5} \frac{\mu}{P} \quad (34)$$

$$k_s = - \frac{J_s V \mu}{dP/dt} = \zeta_{ms} D_s \frac{C_s RT \mu}{P^2 M} \quad (35)$$

Eq. (32) has been validated through molecular simulation and experimental data [39,49]. The model includes the effects of rarefaction, slippage, poromechanical response, nanopore structure (porosity, pore size, surface roughness, and tortuosity), and sorption-induced-swelling response on the bulk-gas transfer. It can successfully describe the contributions of each gas transfer mechanism taking into account the impact of Knudsen diffusion and slip-flow on bulk gas transfer. Notably, it includes the contribution of surface diffusion which is considered as an essential mechanism for transport in the nanopores of shale reservoirs.

3. Methods

3.1. Experimental method

Marcellus Shale samples were used as the reference material for this study to estimate surface diffusion at a low-pressure condition. Dynamic measurements were made by using a gravimetric method. Kinetic gas uptake data were obtained from a gravimetric analyser (Hiden XEMIS) using a sensitive microbalance (see Fig. 2), which measured the change in weight of a shale sample subjected to a step change in adsorbate concentration.

Marcellus shale samples were initially degassed at 383 K overnight to remove the atmospheric moisture. Then, the sample is brought to the adsorption temperature (328 K), chosen to be similar to the actual reservoir conditions used in the simulations. The reservoir temperature is achieved by immersing the adsorbent in an isothermal water bath. Thereafter, adsorption initiates where the adsorbent was exposed to adsorbate gas which passes through the ceramic tube. With sufficiently long adsorption times and monitoring of the sample weight change, constant mass was determined indicating that equilibrium had been attained. Then, the sample was degassed at elevated temperature in order to desorb the gas that was initially injected. By repeating this procedure for a series of various bulk concentrations, a series of uptake curves was generated. Lastly, the uptake curves were corrected for buoyancy effects.

Table 1
Reservoir and fracture parameters for the Marcellus Shale well [29].

Parameter	Value
Initial reservoir pressure, psi	5100
Reservoir Temperature, K	328
Reservoir permeability, nD	800
Reservoir porosity, upper layer	7.1%
Reservoir porosity, bottom layer	14.2%
Initial water saturation	10%
Total compressibility, psi^{-1}	3×10^{-6}
Number of stages	16
Cluster spacing, ft	50
Gas specific gravity	0.58
Fracture height, ft	95
Fracture conductivity, md-ft	3.5
Fracture half-length, ft	400
Total number of fractures	64

Table 2
Parameters of the multicomponent Langmuir isotherm model for adsorption of CH_4 and CO_2 for shales taken from the various stated areas of the Marcellus shale reservoir.

Region of Marcellus	CH_4			CO_2		
	$P_1(\text{psi})$	$V_1(\text{scf/ton})$	$b_1(1/\text{psi})$	$P_1(\text{psi})$	$V_1(\text{scf/ton})$	$b_1(1/\text{psi})$
Oatka	2833	209.0	0.000353	1155	283.5	0.000866
Bedford	1209	133.5	0.000827	1116	352.1	0.000896
Burlington	4771	26.3	0.000210	2951	93.1	0.000339
Canoga	1027	283.5	0.000974	326	360.0	0.003068

3.2. Numerical reservoir simulation method

In this study, the main tool that is used for simulating CO_2 injection is the GEM simulator, which is the CMG (Computer Modelling Group) advanced general equation-of-state compositional simulator [64]. First, a single porosity (SP) model, as proposed by Yu et al. [29] without considering the gas-desorption effect, was generated.

However, the model did not consider the natural fracture system which is crucial for CO_2 injection. Previous studies showed that, actually, a dual permeability model in unconventional reservoirs offers the best prediction of production performance, and yields more reliable outcomes for shale reservoir analysis [65–67]. Hence, for the base case,

a dual porosity dual-permeability model (DP-DP) was developed by keeping constant the main parameters from the SP model (Table 1) and adding natural fracture porosity and permeability. Subsequently, flow via matrix and fractures to the production well, were considered. Once the DP-DP numerical model was history matched with existing field data, then the adsorption capacity from different areas of Marcellus shale was included (Table 2). The corrections presented in section 2.1 were also applied to avoid overestimation of the volume of free gas and the original gas in place.

3.2.1. Basic reservoir model

A commercial simulator (CMG-GEM) was used for the numerical modelling and the analysis of CO_2 injection into the shale reservoirs. The basic 3-dimensional DP-DP model for the Marcellus reservoir (see Fig. 3) was constructed via history matching with existing field scale gas production data published by Chief Oil and Gas LLC [29], using CMG-MOST [64]. Fracture half-length, fracture conductivity, and fracture height were the main tuning parameters used to obtain a good history match (Table 3). After extensive numerical simulations, the best match obtained for the cumulative gas production data has only 0.7% of average matching error (see Fig. 4). Similar to previous researchers, the flowing BHP [29] was utilised to constrain the reservoir simulation.

The field reservoir dimensions are 6000 ft \times 1500 ft \times 130 ft (i.e. length, width and thickness respectively), and there are two shale layers

Table 3
Optimised reservoir and fracture parameters obtained from history matching.

Parameters	Regions of Marcellus				
	No desorption	Oatka	Bedford	Burlington	Canoga
Reservoir Temperature, K	328	328	328	328	328
Matrix permeability, nD	800	800	800	800	800
Fracture permeability, nD	1000	1000	1000	1000	1000
Fracture height, ft	95	70	80	78	80
Fracture half length, ft	350	235	325	325	350
Fracture conductivity, md-ft	3.5	1.5	4	3.7	4.6

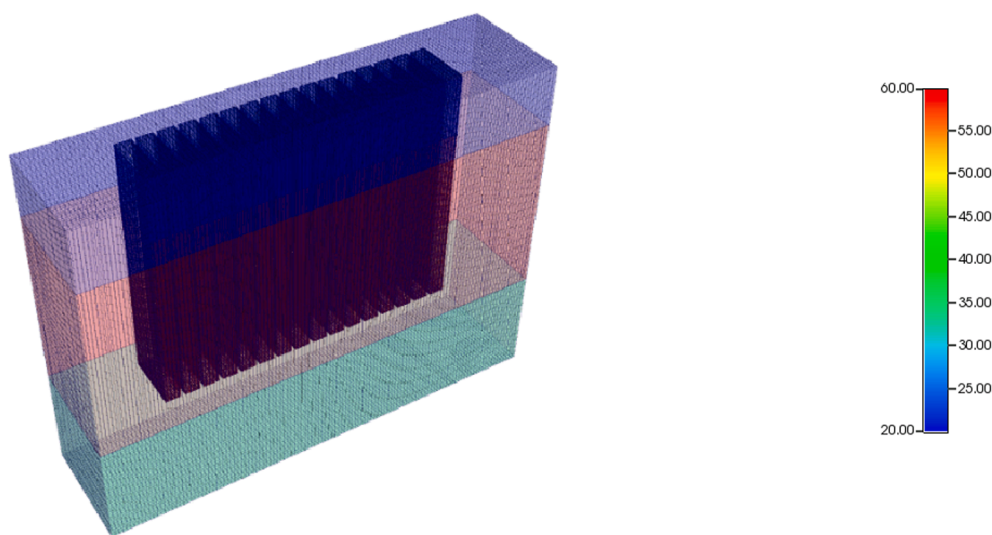


Fig. 3. Schematic view of the DP-DP model of Marcellus shale reservoir. The dark blue area and the colour variation represent hydraulic fractures and reservoir thickness (ft), respectively. The scale bar is the reservoir thickness (ft). (For interpretation of the references to colour in this figure legend, the reader is referred to the web version of this article.)

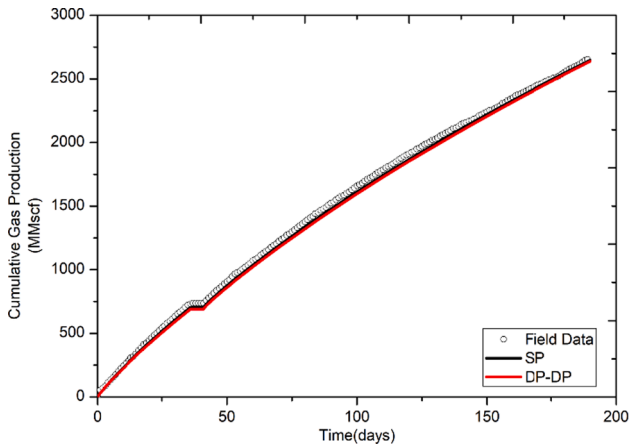


Fig. 4. Comparison between field data (symbols) for cumulative gas production and simulation data (lines) of SP model and DP-DP model.

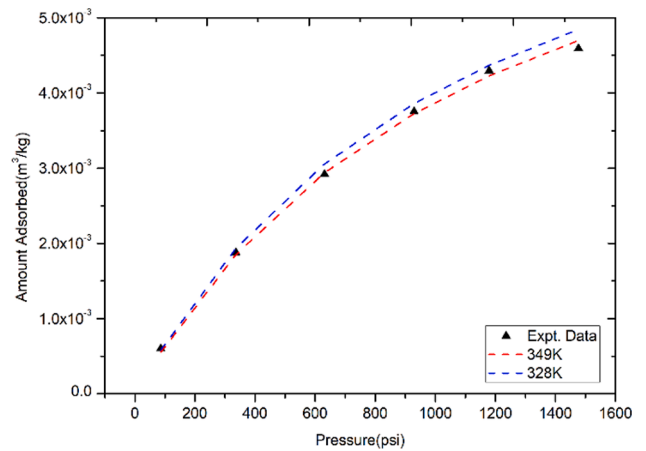


Fig. 7. Experimentally (Expt.) measured adsorption data (symbols) for CO₂ on shale from the Oatka area of the Marcellus shale at temperature of 349 K. Also shown (dashed lines) are fits of the combined Langmuir-Freundlich isotherm model.

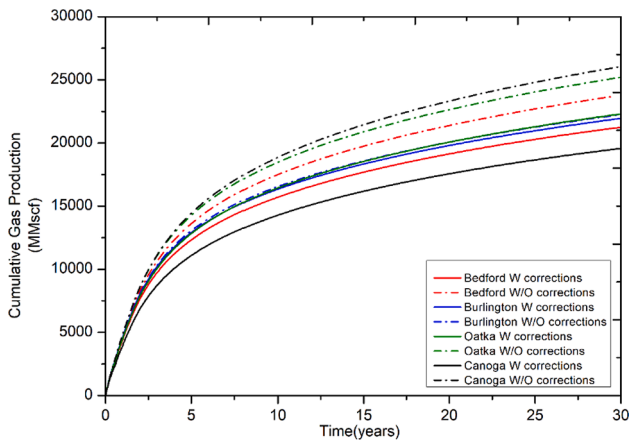


Fig. 5. Comparison of predictions of cumulative gas production performance carried out both with (W) and without (W/O) corrections proposed by Wang et al. [38].

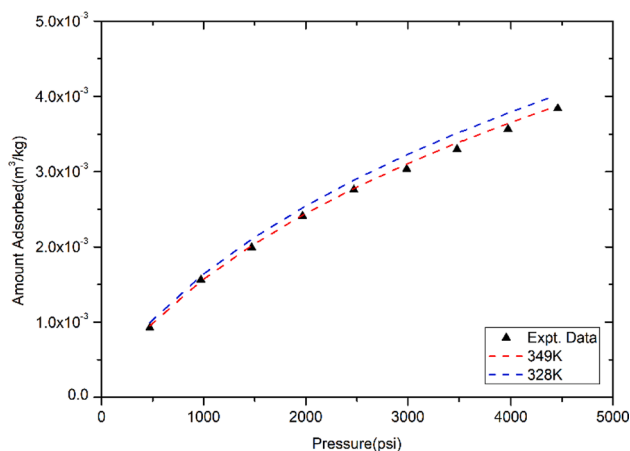


Fig. 6. Experimentally (Expt.) measured adsorption data (symbols) for CH₄ on Oatka area of Marcellus shale at temperature of 349 K. Also shown (dashed lines) are fits of the combined Langmuir-Freundlich isotherm model.

in the reservoir (the upper and the bottom layers) whose porosity values are 7.1% and 14.2%, respectively [29]. Stimulation of the horizontal well is done in the bottom layer that contains 16 fracturing stages, as well as four perforation clusters in every stage with a cluster spacing of

about 50 ft in total, such that the length of the well is approximately 3900 ft. It is assumed that the reservoir is homogeneous, where the fractures are spaced evenly with stress independent permeability and porosity. It should be mentioned that the distance between production and injection wells is 775 ft and remains constant for all of the areas within the Marcellus reservoir.

In the subsequent simulation studies, gas adsorption capacity was considered in the DP-DP model for different areas of Marcellus shale. In particular, the shale samples investigated in this study are taken from the areas of Oatka, Canoga, Bedford, and Burlington [6]. Since gas adsorption is to be considered, the petrophysical properties of the models are corrected according to the theory proposed by Wang et al. [38].

In order to correct the total porosity, water saturation, and gas saturation *a priori*, Eqs. (9)–(11) were used, respectively. Fig. 5 shows that, otherwise, gas production leads to an overestimated OGIP without applying formula corrections (Eqs. (9)–(11)) after 30 years. The results in Fig. 5 are in agreement with similar findings by Wang et al. [38], where an overestimation of up to 50% of gas production was observed.

Competitive adsorption of CO₂ and CH₄ on the shales was described using a multi-component Langmuir isotherm. The parameters for this isotherm were obtained from pure component adsorption experiments. The Langmuir constants for CH₄ and CO₂ for the calculation of the competitive sorption mechanism were obtained from experiments on Marcellus shale cores [6]. Since these experiments were performed at different temperatures from the reservoir simulation model, the combined Langmuir-Freundlich model 2 (Eq. (36)) was applied which has been shown to predict successfully the gas adsorption data at multiple temperatures [68] (see Figs. 6 and 7):

$$V = V_L \exp\left(\frac{-q_1}{T}\right) \left(\frac{b_i P^n}{1 + b_i P}\right) \quad (36)$$

where

$$b_i = b_0 \exp\left(-\frac{\Delta H_{ads}}{RT}\right) \quad (37)$$

and where ΔH_{ads} is the heat of adsorption, b_0 is the pre-exponential factor, and q_1 a temperature-independent constant. The Langmuir constants of CH₄ and CO₂ for the calculation of the competitive sorption are presented in Table 2.

Once the gas adsorption capacities with the corrected petrophysical properties were implemented in the base case model (i.e. DP-DP without desorption), separate history matching was performed for all the

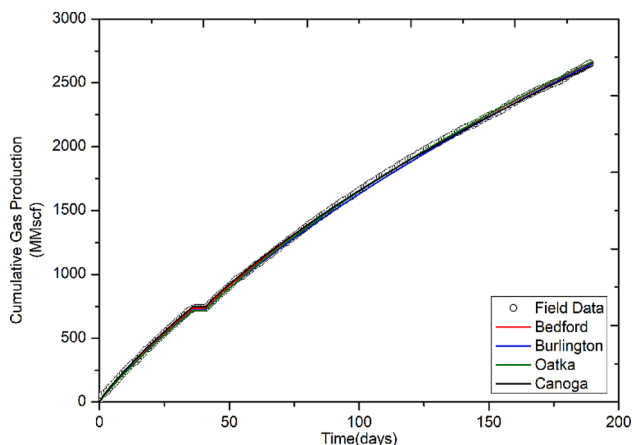


Fig. 8. Comparison between field data (symbols) and simulation results, obtained with Langmuir isotherms, for cumulative gas production from different areas of Marcellus shale reservoir (lines).

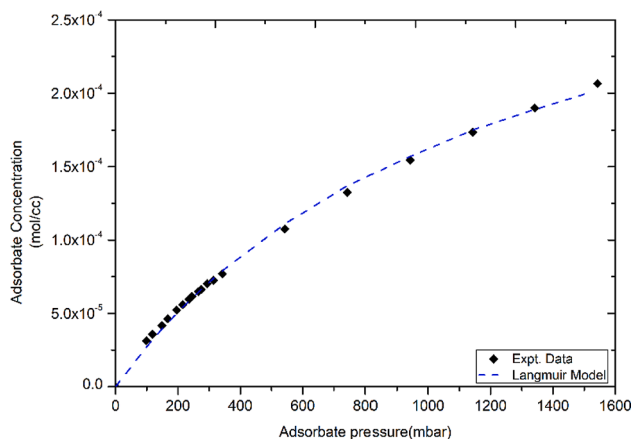


Fig. 9. Equilibrium adsorption data for CO₂ on Marcellus shale at reservoir temperature of 328 K. Also shown (dashed line) a fit of the Langmuir isotherm model. The parameters are given in Table 4.

Table 4

Langmuir isotherm and surface diffusivity parameters obtained from fit of the Do model to CO₂ uptake data for shale samples from Marcellus shale reservoir.

Parameter	Value
Temperature(K)	328
C _{μs} (mol/cm ³)	0.00036
b (cm ³ /mol)	22,188
ε _M	0.076
Ds ₀ (cm ² /sec)	1.3E-07

different areas.

Previous studies have shown that fracture half-length, fracture height, and fracture conductivity are the key parameters to obtain a good history match at the early stage of gas production [29,69]. Thus, history matching was performed by tuning these three parameters. During the history-matching process both fracture height and half-length were reduced relative to the base case model (i.e. DP-DP with no desorption) for each sample (Table 3) from different locales. This observation is in agreement with past findings of previous researchers [29,69] for different regions in Marcellus shale reservoir. As shown in Fig. 8, a good match to the raw adsorption data was obtained using the Langmuir adsorption isotherm for the four samples from the different

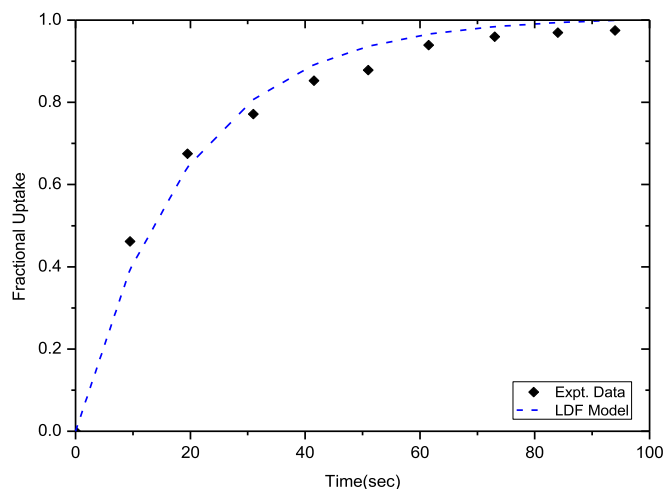


Fig. 10. Experimentally measured (symbols) uptake curves and fits to the LDF mode (dashed line) for CO₂ on Marcellus shale at reservoir temperature of 328 K.

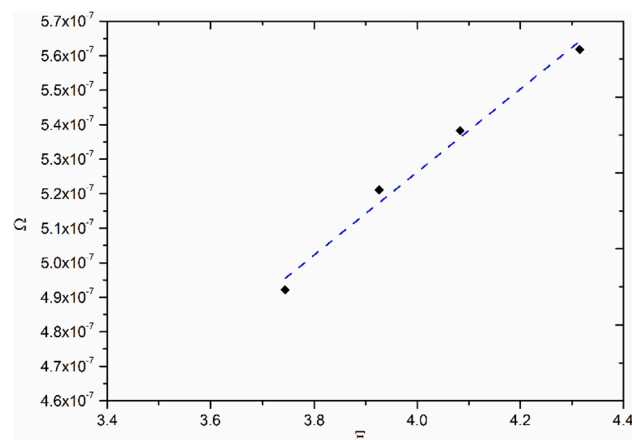


Fig. 11. Plot of Ω versus Ξ for CO₂ for the Marcellus shale reservoir.

areas of the Marcellus reservoir.

4. Results and discussion

4.1. Surface diffusivity

Fig. 9 shows the CO₂ equilibrium isotherm data for a representative sample of the Marcellus shale, obtained at the reservoir temperature (328 K) via the aforementioned gravimetric method. The Langmuir isotherm fits the experimental data well for the reservoir temperature, and the parameters C_{μs} and b, thereby obtained via nonlinear regression are given in Table 4.

The gravimetric kinetic uptake method was used to obtain the variation of fractional uptake of CO₂ with time at 328 K for various bulk concentrations of CO₂ on Marcellus shale. The characteristic half time of the adsorption process was obtained by fitting a single exponential Linear Driving Force (LDF) model to the experimental data. The measured half-time was incorporated into Eq. (19) to estimate the surface diffusivity.

Fig. 10 shows an example of a typical plot of a fit of the experimental data to the Linear Driving Force (LDF) model. Adsorption dynamics were measured at different ultimate bulk gas concentration steps for use in the Do model for surface diffusion.

The experimental uptake data was then fitted to the Do and Rice

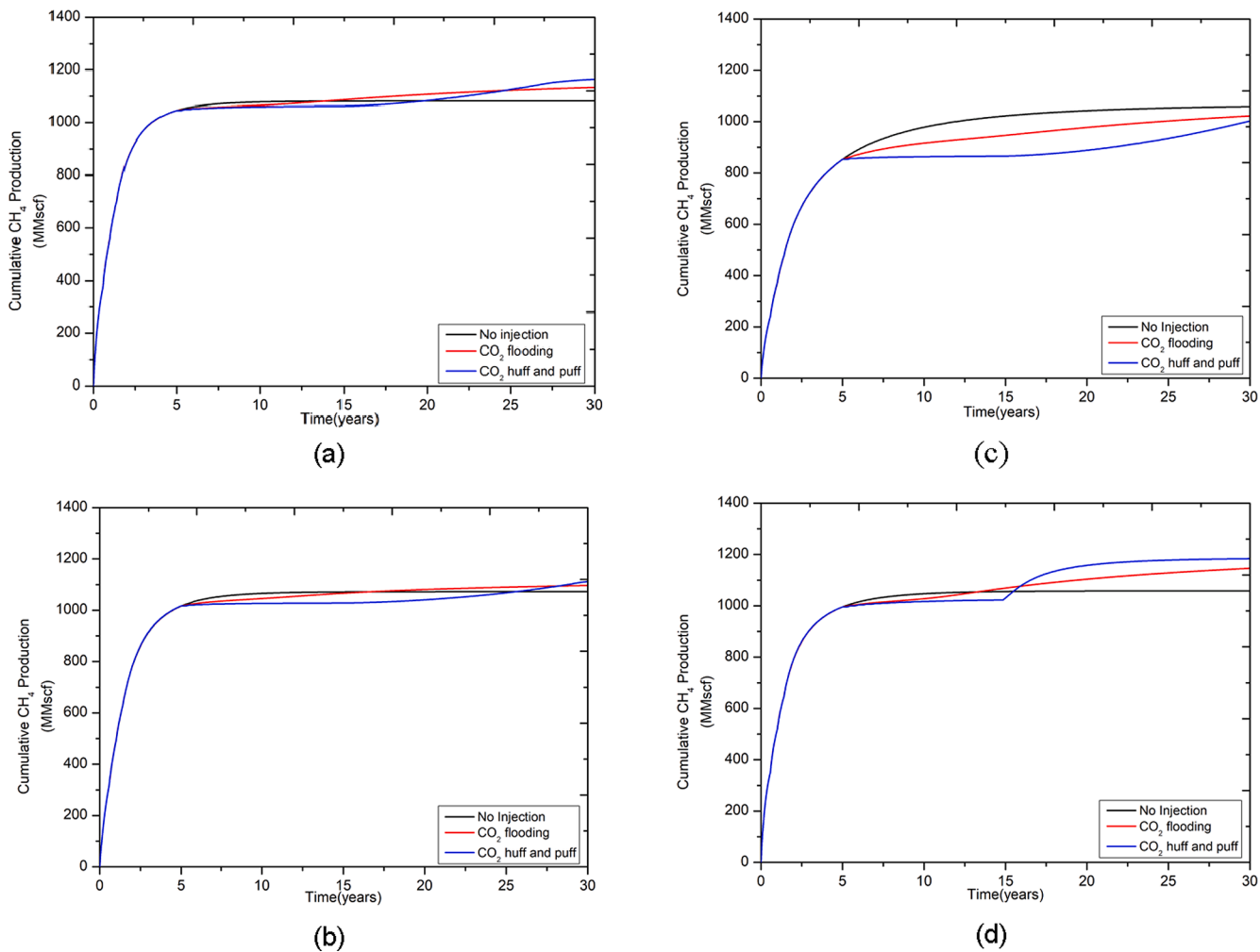


Fig. 12. A comparison of the CH₄ production from the Marcellus shale reservoir with no CO₂ injection, CO₂ flooding, and huff and puff scenarios for the areas of (a) Bedford, (b) Burlington, (c) Oatka, and (d) Canoga.

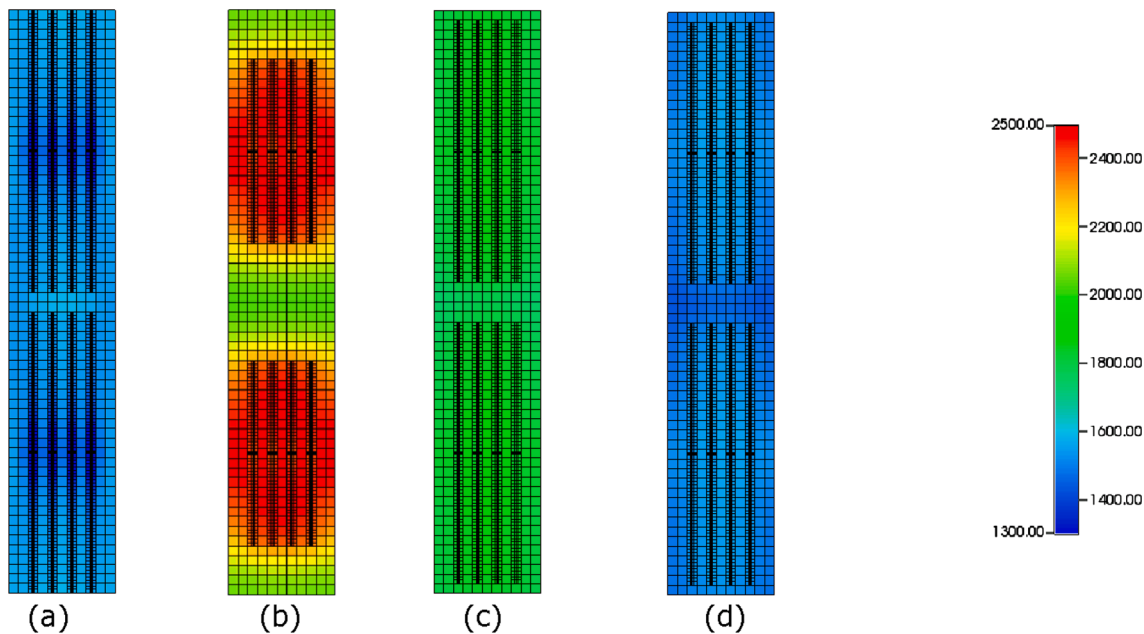


Fig. 13. Distributions of pressure (psi) for the areas of a) Canoga b) Oatka, c) Burlington and d) Bedford of Marcellus shale reservoir at the end of simulation of CO₂ huff and puff after 30 years.

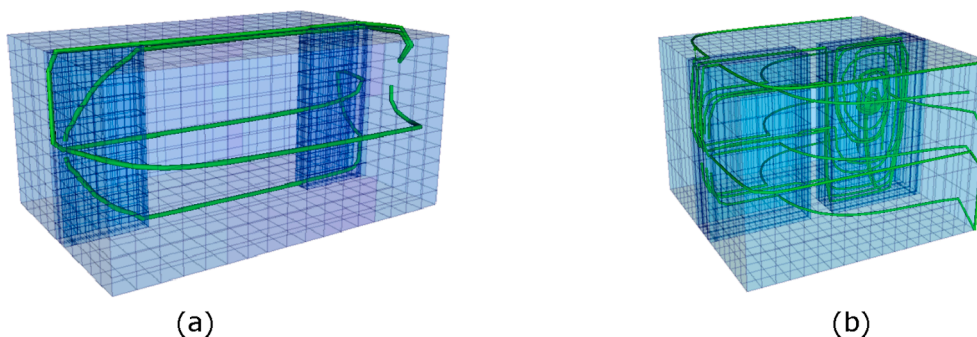


Fig. 14. Schematic views of the a) Barnett and b) New Albany shale reservoirs along with the movement of gas (shown by green lines) at the end of simulation with CO₂ flooding after 30 years. Dark blue areas represent hydraulic fractures. (For interpretation of the references to colour in this figure legend, the reader is referred to the web version of this article.)

Table 5
Reservoir and Fracture parameters for the Barnett and New Albany model.

Parameters	Barnett	New albany
Reservoir Temperature, K	314	303
Porosity	0.029	0.12
Matrix permeability, nD	0.58	150
Natural fracture permeability, nD	7120	1000
Fracture height, ft	330	100
Fracture half length, ft	100	450
Fracture conductivity, md-ft	1	100

Table 6
Parameters of the Langmuir isotherm model for adsorption of CH₄ and CO₂ for shales taken from the Barnett and New Albany shale reservoir.

	CH ₄			CO ₂		
	P _L (psi)	V _L (scf/ton)	b _L (1/psi)	P _L (psi)	V _L (scf/ton)	b _L (1/psi)
Barnett	1596	39.2	0.000627	1254	183.6	0.000797
New Albany	894	119.5	0.001119	1116	510	0.000896

model [59] for surface diffusion. It can be seen from Fig. 11 that the agreement between the experimental data and the linear variation expected from the model of Do and Rice is good. Plotting the parameter Ω , from Eq. (19), versus the parameter Ξ , as shown in Fig. 11, gave rise to a linear form for the data, and a fit to a straight line was used to determine the slope which corresponds to the group $(1-\epsilon_M)D_{so}$.

4.2. Simulation of CO₂ injection scenarios in Marcellus shale reservoir

A simplified segment, for each of the areas of Marcellus shale reservoir, was generated in order to reduce computational demands (Fig. 13). Three different simulation cases have been compared in order

Table 7
Change introduced to production increase percentage (PIP) by adding surface diffusion (SD) after 30 years of production, for the CO₂ flooding scenario. Surface diffusion is estimated via gravimetric experiments (GE) and fractal model (FM), assuming an average pore radius of 0.5 nm, 1 nm, 2 nm.

Regions	PIP (%)					
	0.5 nm		1 nm		2 nm	
	Change With SD (GE)	Change With SD (FM)	Change With SD (GE)	Change With SD (FM)	Change With SD (GE)	ChangeWith SD (FM)
Oatka	1.549	2.996	0.201	0.416	0.040	0.105
Bedford	0.187	0.387	0.019	0.032	0.002	0.003
Burlington	0.340	0.688	0.031	0.075	0.013	0.017
Canoga	1.770	3.167	0.247	0.471	0.048	0.108
Barnett	0.151	0.268	0.025	0.043	0.006	0.010
New Albany	0.908	1.422	0.126	0.197	0.065	0.072

to analyse the effects of different CO₂ injection methods in shale reservoirs, namely no-injection, CO₂ flooding, and CO₂ huff and puff scenarios.

In the case without CO₂ injection, both horizontal wells produce CH₄ for 30 years. Production was conducted by dropping the BHP gradually to 500 psi and maintaining that pressure for 30 years.

In the CO₂ flooding case, both horizontal wells produce shale gas for the first 5 years. After 5 years of production, one well is converted to a CO₂ injector well with a rate of 350 Mscf/day. After 6 years of CO₂ injection, the injector is shut-in, while the other well continues to produce CH₄ for the entire period of 30 years. It should be noted that the carbon dioxide injected is in a supercritical state due to the reservoir conditions.

In the huff and puff case, both horizontal wells produce CH₄ for 5 years, and then both wells are converted to CO₂ injectors with a rate of 640 Mscf/day for 2 months. After a 1 month soaking period, both wells are converted back to producers for 3 months. This cycle is repeated for 10 years and the overall amount of CO₂ injected is the same as for the CO₂ flooding case.

As can be seen from the findings shown in Fig. 12(a–d), CH₄ production for the cases with CO₂ injection is higher than that of the models without CO₂ injection in all areas except for the Oatka area. The reason for this exception is probably due to the combination of a small fracture conductivity value, and the reduced fracture half-length, in Oatka.

In the findings for the Bedford and Canoga areas (in Fig. 12a, b), it can be observed that CH₄ production with CO₂ flooding starts approximately after 8 years. Despite the fact that the sample from the Burlington area has the lowest Langmuir b constant for CH₄, and thus it might be expected that CH₄ is more weakly bound to the shale there, the CH₄ production with CO₂ flooding starts approximately after 12 years. A potential reason, for this apparent anomaly, is a combination of the low fracture conductivity value, along with the low monolayer volume of CH₄ for the Burlington area, when compared to the samples from Bedford and Canoga areas. The cumulative gas production from the Bedford, Canoga, and Burlington areas were 4.8%, 8.3%, and 2.2%, respectively, higher than for the no CO₂ injection model at the end of production.

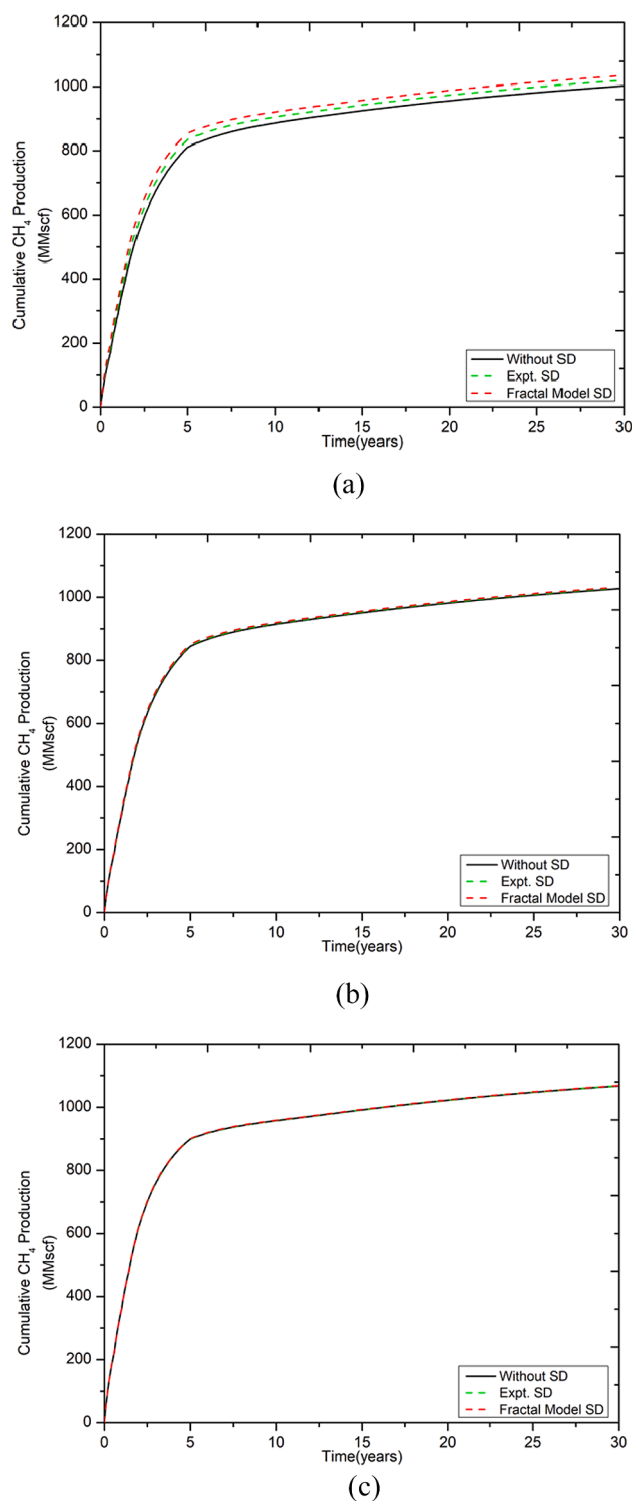


Fig. 15. Cumulative CH₄ production with an average pore radius of a) 0.5 nm, b) 1 nm, and c) 2 nm for the Canoga area with CO₂ flooding scenario.

From Fig. 12d, in the CO₂ huff and puff scenario, it can be observed that a steep increase of CH₄ production occurred once the cycles had been completed in the Canoga area. As shown in Fig. 13, this steep increase is probably due to low reservoir pressure which results from the spread of CO₂ molecules through the reservoir. The CH₄ production for the remaining areas increases more steadily. The cumulative gas production from the Bedford, Canoga, and Burlington areas was 7.7%, 11.9%, and 3.7%, respectively, higher than for the no CO₂ injection case

at the end of production.

4.3. Effects of surface diffusivity

One of the issues yet to be addressed in the literature is that only a few studies have implemented, into a reservoir simulator, an apparent permeability model that includes additional mass transfer mechanisms beyond Darcy flow [26,70,71]. However, even these studies did not include all gas transfer mechanisms, especially surface diffusion, which may result in overestimating, or underestimating, gas production. To the best of our knowledge, this is the first study that extends the established model of Wu et al. [39] for gas transport in nanopores of shale gas reservoirs to include surface diffusion and has implemented it into a reservoir simulator. The basic underlying apparent permeability model (Eq. (32)) has already been validated through experimental data and molecular simulation [39].

Models for the Barnett and New Albany shales have been generated to investigate the effect of CO₂ surface diffusion on CH₄ production compared with other areas from the Marcellus shale reservoir. Fig. 14 shows the geological models of the Barnett and New Albany shale reservoirs used. The models were created based on the reservoir data of Kim et al. [30] and Liu et al. [72], respectively (Table 5). Similar to the approach of previous researchers, both models are segregated for computational efficiency. The parameters of the Langmuir isotherm for adsorption of CH₄ and CO₂ in the two shales implemented in these models have been estimated in previous studies (Table 6) [73,74]. Eq. (22) was applied in order to estimate the surface diffusion at the appropriate temperature of each reservoir.

Eq. (32) was applied to determine the apparent permeability, via permeability multipliers which are functions of pressure, for the different areas of the Marcellus reservoir. Thereafter, evaluation of the impact of surface diffusion on methane recovery was investigated for models with pores in the micropore region (≤ 2 nm) where surface diffusion is more pronounced [39,49]. The variation in typical pore sizes for porous matrices studied in this work is 0.5 nm, 1 nm, and 2 nm, and the surface diffusivity employed in the models was ultimately determined from the gravimetric experiments.

Assuming that the average pore radius is 0.5 nm, in certain regions of the Marcellus shale reservoir, such as the Canoga and Oatka areas, and in the New Albany reservoir, the cumulative CH₄ produced at the end of production, as predicted by the new reservoir simulator models presented here, can range between 0.91% and 1.8% higher than for the equivalent CO₂ injection model without considering surface diffusion (Table 7). However, as the average pore radius increases to 1 nm and 2 nm (Fig. 15b, c), the cumulative CH₄ production declines significantly, which results in a smaller percentage of increase of CH₄ production due to surface diffusion.

Further, the fractal surface diffusion model, implemented via Eqs. (18)–(20), was used to investigate the impact of the particular morphology of the specific shale rock in the Marcellus reservoir on CH₄ production. It should be mentioned that the fractal dimension used in all the marine reservoirs (Marcellus, Barnett, New Albany) investigated is 2.9 and was obtained from the Frenkel-Halsey-Hill (FHH) model applied to N₂ adsorption data [42,75]. For the fractal surface diffusion model in all regions, the production with surface diffusion is higher by up to 1.5%, thereby enhancing further the CH₄ production compared with the model with the experimental surface diffusivity (Table 7).

An improvement in cumulative gas production of the order of 1.5% could still yield 250 (MSCF) of additional gas. It has been reported that 250 (MSCF) could bring in additional revenue of up to \$500,000 with an assumption of a gas price of \$5 per thousand cubic feet and a CO₂ price of \$20 per ton [76].

While the data are not shown, when, for comparison purposes, surface diffusivity was estimated for a shale surface with a low fractal dimension, the results for CH₄ production were similar to the models without surface diffusion. This is probably because a higher surface

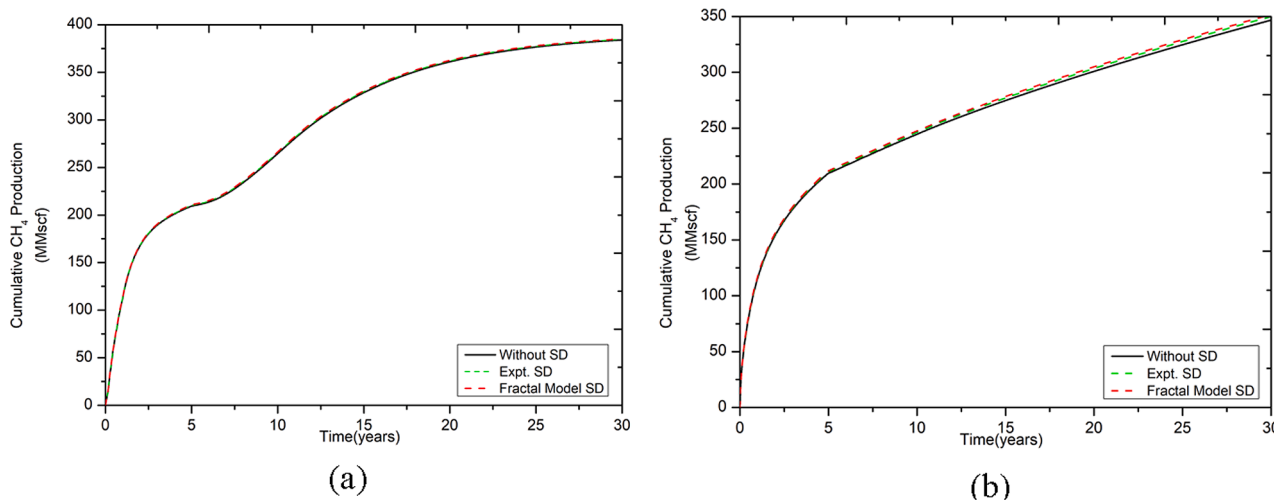


Fig. 16. Cumulative CH₄ production, assuming an average pore radius of 0.5 nm for (a) Barnett and (b) New Albany shale reservoir, for the CO₂ flooding scenario.

Table 8

Change introduced to CO₂ adsorption increase percentage (AIP) molecules by adding surface diffusion (SD) after 30 years of production, for the CO₂ injection scenarios. Surface diffusion is estimated via fractal model (FM), assuming an average pore radius of 0.5 nm, and 1 nm.

Regions	CO ₂ AIP (%)			
	CO ₂ flooding		CO ₂ huff and puff	
	0.5 nm	1 nm	0.5 nm	1 nm
	Change With SD (FM)	Change With SD (FM)	Change With SD (FM)	Change With SD (FM)
Oatka	1.63	0.29	0.63	0.06
Bedford	0.48	0.47	0.53	0.26
Burlington	1.32	0.23	1.35	0.55
Canoga	2.74	1.06	0.73	0.71
Barnett	0.20	0.02	1.19	0.24
New Albany	1.22	0.29	2.04	1.41

Table 9

Change introduced to CH₄ desorption increase percentage (DIP) molecules by adding surface diffusion (SD) after 30 years of production, for the CO₂ injection scenarios. Surface diffusion is estimated via fractal model (FM), assuming an average pore radius of 0.5 nm, and 1 nm.

Regions	CH ₄ DIP (%)			
	CO ₂ flooding		CO ₂ huff and puff	
	0.5 nm	1 nm	0.5 nm	1 nm
	Change With SD (FM)	Change With SD (FM)	Change With SD (FM)	Change With SD (FM)
Oatka	2.37	0.33	3.31	0.48
Bedford	0.51	0.05	0.77	0.04
Burlington	0.57	0.06	1.13	0.17
Canoga	2.29	0.33	2.61	0.36
Barnett	0.71	0.20	2.05	0.26
New Albany	1.46	0.21	1.32	0.19

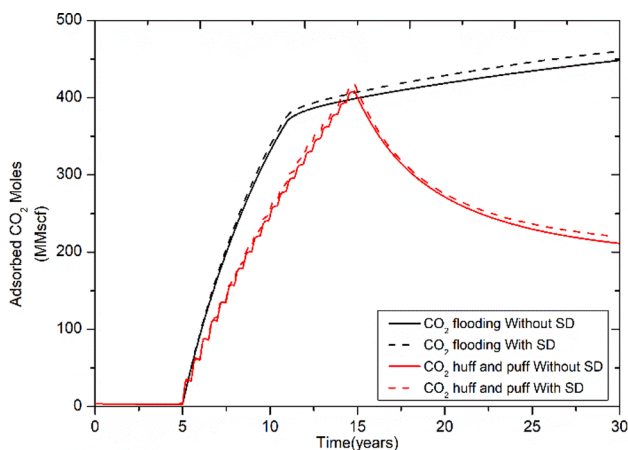


Fig. 17. Effect of inclusion of surface diffusion (SD), assuming an average pore radius of 0.5 nm, on the amount of adsorbed CO₂ molecules for the Canoga area with CO₂ flooding and CO₂ huff and puff scenario.

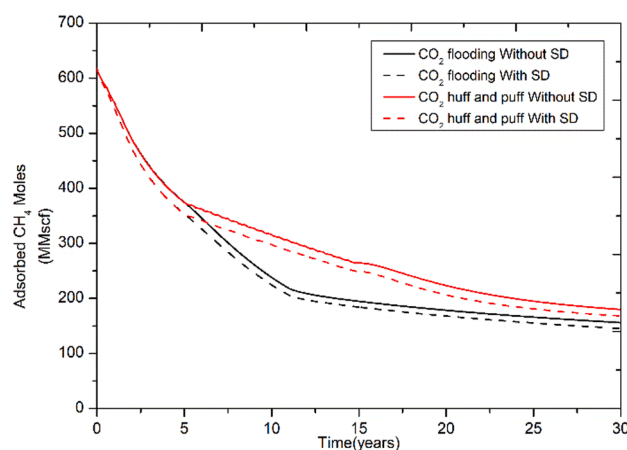


Fig. 18. Effect of surface diffusion (SD), assuming an average pore radius of 0.5 nm, on comparison of remaining adsorbed CH₄ molecules for the Canoga area with a) CO₂ flooding and b) CO₂ huff and puff scenario.

fractal dimension will enhance surface diffusion significantly. It should be noted that surface diffusion at similar pore radii was also investigated for the huff and puff scenario and the results for the cumulative CH₄ production were similar to those for CO₂ flooding.

From Table 7, it can be seen that the contribution of SD to PIP

becomes less pronounced with an increase of typical pore radius in all the reservoirs examined. This result is reasonable considering that the smaller the pore radius, the greater the ratio of surface area per unit volume, and, thus the greater adsorbed-gas transfer volume via surface diffusion. In addition, it has been observed that the apparent

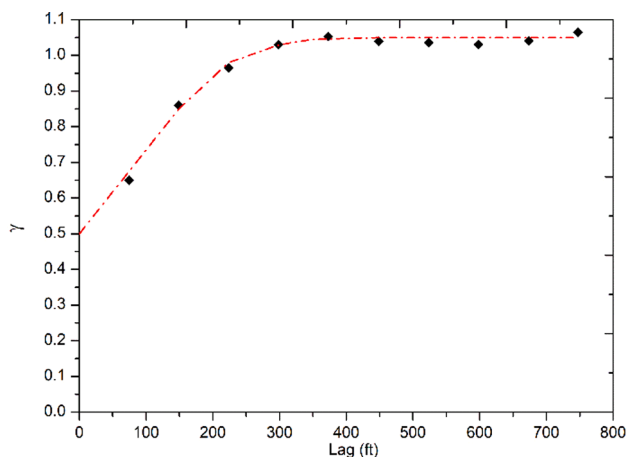


Fig. 19. Spherical model (dashed line) with a nugget value of 0.5 fitted to the generated permeability data (symbols) for a semivariogram model. The semivariogram model represents the Canoga area of Marcellus shale reservoir.

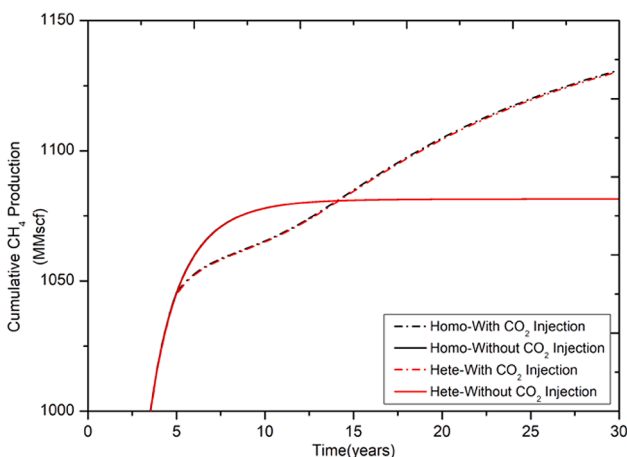


Fig. 20. Effect of spatial heterogeneities in reservoir permeability on CH₄ production over time in cases with and without CO₂ injection for the area of Bedford (Homo:Homogeneous case, Hete:Heterogeneous case).

permeability of surface diffusion decreases with an increase in pressure. From Eq. (35), the apparent permeability of surface diffusion is related not only to the surface-diffusion coefficient but also to the ratio of the adsorbed-gas concentration to the square of reciprocal pressure C_s/p^2 . This means that, the ratio of the adsorbed-gas concentration to the square of reciprocal pressure is greater than the increase of the surface diffusion coefficient which results in a low surface diffusion flux.

Comparing the findings for the Bedford area of the Marcellus reservoir, and for the Barnett shale (Fig. 16a) reservoir, to the corresponding findings for New Albany (Fig. 16b) and the remaining areas of Marcellus shale reservoir (i.e. Canoga, Burlington, Oatka), it can be seen that surface diffusion does not make an important contribution to gas transfer, and, thus to CH₄ production (Table 7). The reason for this insignificant contribution of surface diffusion to CH₄ production in certain areas, is that the surface capacity in those areas is lower. Surface diffusion becomes more pronounced when the surface capacity is higher since this means a greater amount of adsorbed gas molecules. Hence, the values of the Langmuir capacity parameter play a critical role in determining the effectiveness of CO₂ injection and should be considered in shale gas reservoirs.

Table 8 shows the variation in the amount of adsorbed CO₂ molecules, for each of the CO₂ injection scenarios, when compared to the equivalent CO₂ injection models without considering surface diffusion.

The results indicate that the effect of surface diffusion on the CO₂ amount adsorbed is not significant for the regions that have low surface capacity. The Canoga region of the Marcellus shale reservoir has the highest surface capacity and, in the flooding scenario, the amount of adsorbed CO₂ molecules may increase by up to 2.74% when surface diffusion is included and the average pore radius is 0.5 nm (Fig. 17).

Fig. 17 also shows the variation in the amount of adsorbed CO₂ for the huff and puff scenario. The results indicate that the relative increase in the amount of adsorbed CO₂ molecules for the models with surface diffusion compared to no surface diffusion, is similar to those for the CO₂ flooding scenario. It should be mentioned that, in the case of the CO₂ huff and puff scenario, the total amount of CO₂ molecules trapped in the reservoir is roughly half the amount of CO₂ molecules trapped in the flooding scenario. The reason for the observed difference between the two injection scenarios is that the CO₂ molecules cannot spread as far within the reservoir during the huff and puff method, since CO₂ is produced during the puff cycles.

Table 9 shows the variation in the amount of desorbed CH₄ molecules for the various CO₂ injection scenarios compared to the equivalent CO₂ injection models without considering surface diffusion. In areas with high surface capacity, such as Canoga (Fig. 18) and Oatka, when surface diffusion is applied, the amount of desorbed CH₄ molecules may increase by up to 2.3% in the flooding scenario. In the remaining areas, the effect of surface diffusion on the amount of CH₄ desorbed molecules is not significant. This result is similar to the effect of surface diffusion on the amount of CO₂ adsorbed molecules.

Fig. 18 also shows the variation over time of the adsorbed amount of CH₄ for the Canoga area of the Marcellus shale reservoir during CO₂ huff and puff. In all reservoirs investigated, the difference between the corresponding amounts of CH₄ desorbed for the models with surface diffusion and without surface diffusion is similar to found for the CO₂ flooding scenario.

The results indicate that the amount of CH₄ desorbed is always higher in the case of the CO₂ flooding technique when compared to huff and puff, except for the case of the New Albany reservoir. A reason for the higher amount of CH₄ desorbed in the huff and puff scenario is the high fracture conductivity of the New Albany reservoir (Table 9) which exhibits a wider-spread of CH₄ molecules within the reservoir. In particular, the model that has the lowest fracture conductivity (Oatka) shows the largest difference in CH₄ amount desorbed amongst the various CO₂ injection techniques (i.e. CO₂ flooding and huff and puff).

4.4. Effect of reservoir heterogeneity

Geostatistics is defined as a technique which takes into consideration spatial relationships of variables in estimating values of the variables at unsampled locations. Geostatistical modelling assumes that reservoir properties (i.e. porosity, permeability) are more similar at two nearby locations than for two locations distant from each other. In this work, a geostatistical approach was used for stochastically generating multiple permeability realizations to assess the effect of reservoir heterogeneity on gas production.

The observed statistical data on permeability, namely the variance and mean, are utilised in the stochastic method, in conjunction with correlation lengths representing model anisotropy in various directions. This means that this approach generated a relationship between permeability and distance, from a given site, and thus was capable of representing the natural variability of permeability. In addition, the geostatistical approach helps in quantifying uncertainty when describing the reservoir.

Hereafter, semivariogram modelling is used, which is mathematically defined as a measure of dissimilarity over distance. A semivariogram model expresses the generated permeability data and captures the correlation between the spatial variation of the permeability with distance. In particular, the spherical semivariogram is applied to describe the generated heterogeneity, since it has been shown to be the best fit to

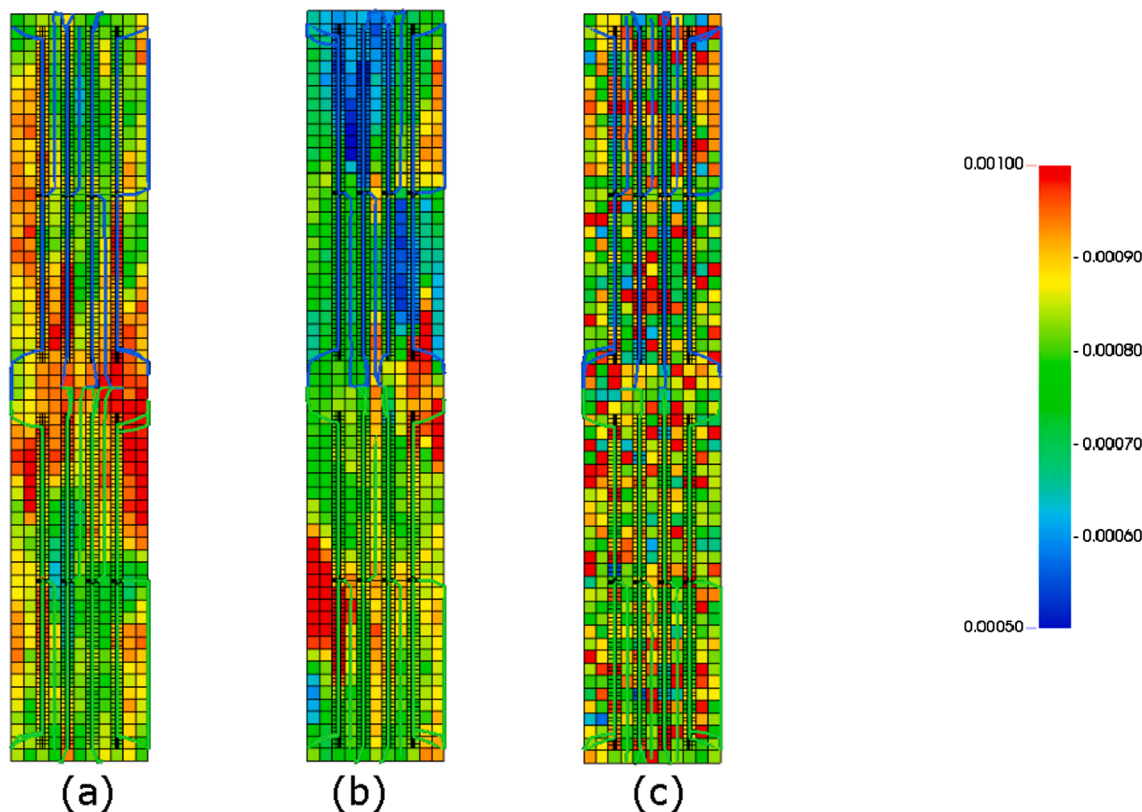


Fig. 21. Maps of 2D sections through reservoir models with heterogeneity in the spatial distribution of permeability exhibiting either (a) minimum heterogeneity or (b) medium heterogeneity or (c) maximum heterogeneity along with the movement of gas (shown by The flowlines) with CO₂ flooding at the end of simulation. The scale bar is the permeability (mD).

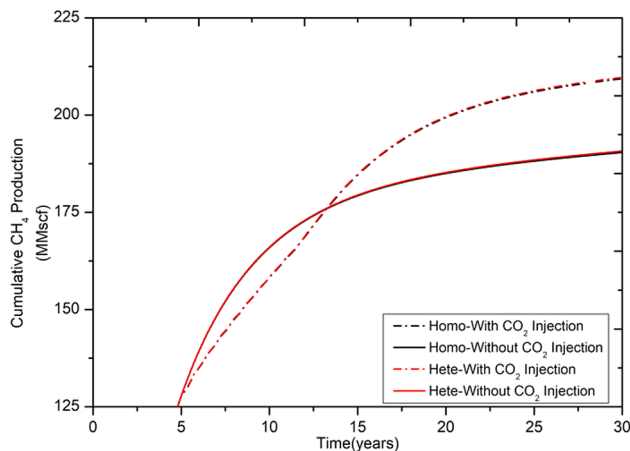


Fig. 22. Effect of reservoir permeability on comparison on CH₄ production with and without CO₂ injection for Barnett shale reservoir (Homo:Homogeneous case, Hete:Heterogeneous case).

experimental variograms for shales [15,77]. From Fig. 19 it can be seen that the semivariance (γ) increases as a function of separation distance (lag). For instance, γ shows smaller permeability values for paired samples which are closer together in space. However, the difference between permeability data increases with lag.

Discontinuities in the spatial distribution of permeability data within the reservoir are generated using the nugget effect. The nugget effect adds an amount of short-wavelength randomness to the solution from Geostatistics. In particular, a nugget is the vertical jump from the value of zero at the origin (0 lag) to the value of the variogram. More heterogeneity and increased discontinuities are caused by a larger value of

the nugget.

Fig. 20 shows the comparison between methane gas production, with and without CO₂ injection, for cases of heterogeneous and homogeneous reservoir models for the Bedford area. Different nugget values of 0.001, 0.01 and 0.5 were used in this work to represent minimum, medium and maximum heterogeneity respectively (as shown in Fig. 21). In the three heterogeneous reservoir model with different nugget values, the average permeability is similar to the base case of each reservoir.

After a production period of 30 years, the incremental CH₄ production, for all the areas in the Marcellus shale reservoir considered in the heterogeneous case, is less than for the homogeneous base case. The overall percentages produced of original CH₄ in-place for minimum, medium and maximum levels of heterogeneity are lower compared to the homogeneous base case by approximately 0.8%, 1.2% and 1.5% respectively. Similarly to Marcellus shale reservoir, the CH₄ production from the New Albany shale for minimum, medium and maximum levels of heterogeneity are lower compared to the homogeneous base case by approximately 0.01%, 0.05% and 0.07% respectively. A reason for the reduction in the produced CH₄ in-place in the heterogeneous case, may be because of the slower mass transport rates than for the homogeneous case. This results in a greater amount of CO₂ trapped in the matrix which inhibits gas migration.

In contrast, the results for the Barnett shale reservoir shown in Fig. 22 exhibit a small increase in CH₄ production in the case of heterogeneity in permeability. The data in Fig. 22 shows that the CH₄ production values for minimum, medium and maximum degrees of heterogeneity in permeability are relatively higher than for the homogeneous base case by approximately 0.02%, 0.05% and 0.1% respectively. In contrast to the homogeneous base case model for the Barnett reservoir, adding heterogeneity enhances the CO₂ flow to the production well. It should be noted that Barnett shale has a lower overall permeability compared to the New Albany and Marcellus shale reservoirs. The

new higher permeability sites introduced by the heterogeneous model assist mass transport relative to the uniformly low permeability in the homogeneous case thereby enhancing CH₄ production. The corresponding results for simulations of the impact of spatial heterogeneities in permeability on the performance of the huff and puff technique are similar to those for CO₂ flooding.

5. Conclusion

In the areas of Bedford, Canoga, and Burlington of the Marcellus shale reservoir, there is an increase of CH₄ production by CO₂ injection compared to no injection scenario due to high fracture conductivity. It has been shown that the surface diffusivity estimated from gravimetric experiments makes an important contribution to CH₄ production when the average pore radius is less than 2 nm and should not be ignored. It has also been found that a high fractal dimension (2.9) may enhance CH₄ production when the average pore radius is less than 1 nm. For example, when the average pore size is 0.5 nm, areas with high surface capacity show an increase up to 3.2% of cumulative gas production when surface diffusion is applied. This increase could bring a revenue by up to \$1 million with an assumption of gas price \$5 per thousand cubic feet and CO₂ price \$20 per ton. In the remaining reservoirs, surface diffusion is not pronounced since the ratio of the adsorbed-gas concentration to the square of pressure is greater than the increase of surface diffusion coefficient.

The effect of surface diffusion on the amount of CO₂ molecules adsorbed and CH₄ molecules desorbed is not significant for the regions that have low surface capacity. However, for areas with high surface capacity, such as Canoga, adsorption of CO₂ and desorption of CH₄ molecules may increase by up to 2.74% and 2.3%, respectively, when compared to the models with no surface diffusion.

In all the areas investigated, geostatistical simulations showed that reservoir heterogeneity is not favourable for the CO₂ injection techniques, except the Barnett shale reservoir. The reason for this exception is probably due to the impact of high permeability heterogeneities in an otherwise low permeability of the reservoir (0.58 nD) which results in the CO₂ diffusion being more pronounced, and, thus enhancing CH₄ production.

CRedit authorship contribution statement

Dimitris Spanakos: Methodology, Software, Validation, Formal analysis, Investigation, Writing – original draft, Visualization. **Sean P. Rigby:** Conceptualization, Resources, Writing - review & editing, Supervision.

Declaration of Competing Interest

The authors declare that they have no known competing financial interests or personal relationships that could have appeared to influence the work reported in this paper.

Acknowledgements

The authors are grateful for the support from Computer Modelling Group (CMG) for supplying the simulation software and technical assistance. This work was supported by the Engineering and Physical Sciences Research Council (EPSRC) [Grant Reference number EP/N50970X/1].

References

- Lozano-Maya JR. Looking through the prism of shale gas development: Towards a holistic framework for analysis. *Energy Res Soc Sci* 2016;20:63–72. <https://doi.org/10.1016/j.erss.2016.05.014>.
- Wang J, Yuan Q, Dong M, Cai J, Yu L. Experimental investigation of gas mass transport and diffusion coefficients in porous media with nanopores. *Int J Heat Mass Transf* 2017;115:566–79. <https://doi.org/10.1016/j.ijheatmasstransfer.2017.08.057>.
- International Energy Agency. World Energy Outlook 2017.
- Yuan J, Luo D, Feng L. A review of the technical and economic evaluation techniques for shale gas development. *Appl Energy* 2015;148:49–65. <https://doi.org/10.1016/j.apenergy.2015.03.040>.
- Weijermars R. US shale gas production outlook based on well roll-out rate scenarios. *Appl Energy* 2014;124:283–97. <https://doi.org/10.1016/j.apenergy.2014.02.058>.
- Dilmore R, Bruner K, Wyatt C, Romanov V, Goodman A, Hedges S, et al. Experimental Characterization of Marcellus Shale Outcrop Samples, and Their Interactions with Carbon Dioxide and Methane. U.S. Dep Energy, Natl Energy Technol Lab Morgantown, WV NETL Tech Rep Ser 2015. <https://doi.org/10.18141/1432659>.
- Abedini A, Torabi F. On the CO₂ storage potential of cyclic CO₂ injection process for enhanced oil recovery. *Fuel* 2014;124:14–27. <https://doi.org/10.1016/j.fuel.2014.01.084>.
- Pan Z, Connell LD. Reservoir simulation of free and adsorbed gas production from shale. *J Nat Gas Sci Eng* 2015;22:359–70. <https://doi.org/10.1016/j.jngse.2014.12.013>.
- Yuan W, Pan Z, Li X, Yang Y, Zhao C, Connell LD, et al. Experimental study and modelling of methane adsorption and diffusion in shale. *Fuel* 2014;117:509–19. <https://doi.org/10.1016/j.fuel.2013.09.046>.
- Louk K, Ripepi N, Luxbacher K, Gilliland E, Tang X, Keles C, et al. Monitoring CO₂ storage and enhanced gas recovery in unconventional shale reservoirs: results from the Morgan County, Tennessee injection test. *J Nat Gas Sci Eng* 2017;45:11–25. <https://doi.org/10.1016/j.jngse.2017.03.025>.
- Nuttal BC, Eble C, Bustin RM, Drahovzal JA. Analysis of Devonian black shales in Kentucky for potential carbon dioxide sequestration and enhanced natural gas production. *Greenh Gas Control Technol Elsevier Ltd* 2005:2225–8. <https://doi.org/10.1016/B978-008044704-9/50306-2>.
- Fathi E, Akkutlu IY. Multi-component gas transport and adsorption effects during CO₂ injection and enhanced shale gas recovery 2014. 10.1016/j.coal.2013.07.021.
- Heller R, Zoback M. Adsorption of methane and carbon dioxide on gas shale and pure mineral samples. *J Unconv Oil Gas Resour* 2014;8:14–24. <https://doi.org/10.1016/j.juogr.2014.06.001>.
- Li X, Elsworth D. Geomechanics of CO₂ enhanced shale gas recovery. *J Nat Gas Sci Eng* 2015;26:1607–19. <https://doi.org/10.1016/j.jngse.2014.08.010>.
- Yu W, Lashgari HR, Wu K, Sepehrnoori K. CO₂ injection for enhanced oil recovery in Bakken tight oil reservoirs. *Fuel* 2015;159:354–63. <https://doi.org/10.1016/j.fuel.2015.06.092>.
- Kim J, Maiti A, Lin L-C, Stolaroff JK, Smit B, Aines RD. New materials for methane capture from dilute and medium-concentration sources. *Nat Commun* 2013;4:1694. <https://doi.org/10.1038/ncomms2697>.
- Busch A, Alles S, Gensterblum Y, Prinz D, Dewhurst D, Raven M, et al. Carbon dioxide storage potential of shales. *Int J Greenh Gas Control* 2008;2:297–308. <https://doi.org/10.1016/j.jggc.2008.03.003>.
- Shi J-Q, Durucan S. Modelling of mixed-gas adsorption and diffusion in coalbed reservoirs. *SPE Unconv Reserv Conf, Society of Petroleum Engineers* 2008. <https://doi.org/10.2118/114197-MS>.
- Crosdale PJ, Beamish BB, Valix M. Coalbed methane sorption related to coal composition. *Int J Coal Geol* 1998;35:147–58. [https://doi.org/10.1016/S0166-5162\(97\)00015-3](https://doi.org/10.1016/S0166-5162(97)00015-3).
- Curtis JB. Fractured shale-gas systems. *Am Assoc Pet Geol Bull* 2002;86:1921–38. <https://doi.org/10.1306/61EEDDBE-173E-11D7-8645000102C1865D>.
- Pan Z, Wood DA. Coalbed methane (CBM) exploration, reservoir characterisation, production, and modelling: a collection of published research (2009–2015). *J Nat Gas Sci Eng* 2015;26:1472–84. <https://doi.org/10.1016/j.jngse.2015.07.049>.
- Chalmers GRL, Marc BR. On the effects of petrographic composition on coalbed methane sorption. *Int J Coal Geol* 2007;69:288–304. <https://doi.org/10.1016/j.coal.2006.06.002>.
- Zhang T, Ellis GS, Ruppel SC, Milliken K, Yang R. Effect of organic-matter type and thermal maturity on methane adsorption in shale-gas systems. *Org Geochem* 2012;47:120–31. <https://doi.org/10.1016/j.orggeochem.2012.03.012>.
- Ross DJK, Bustin RM. Shale gas potential of the lower jurassic gordondale member, northeastern British Columbia, Canada. *Bull Can Pet Geol* 2007;55:51–75. <https://doi.org/10.2113/gscpgbull.55.1.51>.
- Lu X, Jin D, Wei S, Zhang M, Zhu Q, Shi X, et al. Competitive adsorption of a binary CO₂–CH₄ mixture in nanoporous carbons: effects of edge-functionalization. *Nanoscale* 2015;7:1002–12. <https://doi.org/10.1039/C4NR05128A>.
- Wang J, Liu H, Yu W, Cao F, Sepehrnoori K. Necessity of porosity correction before simulation and re-understanding of the effects of gas adsorption on production in shale gas reservoirs. *J Pet Sci Eng* 2016;139:162–70. <https://doi.org/10.1016/j.petrol.2015.12.022>.
- Xiong J, Liu X, Liang L, Zeng Q. Methane adsorption on carbon models of the organic matter of organic-rich shales. *Energy Fuels* 2017;31:1489–501. <https://doi.org/10.1021/acs.energyfuels.6b03144>.
- Firouzi M, Rupp EC, Liu CW, Wilcox J. Molecular simulation and experimental characterization of the nanoporous structures of coal and gas shale. *Int J Coal Geol* 2014;121:123–8. <https://doi.org/10.1016/j.coal.2013.11.003>.
- Yu W, Sepehrnoori K, Patzek TW. Modeling gas adsorption in marcellus shale with langmuir and BET isotherms. *SPE J* 2016;21:589–600. <https://doi.org/10.2118/170801-PA>.

- [30] Kim TH, Cho J, Lee KS. Evaluation of CO₂ injection in shale gas reservoirs with multi-component transport and geomechanical effects. *Appl Energy* 2017;190:1195–206. <https://doi.org/10.1016/j.apenergy.2017.01.047>.
- [31] Zhong J, Abedini A, Xu L, Xu Y, Qi Z, Mostowfi F, et al. Nanomodel visualization of fluid injections in tight formations. *Nanoscale* 2018;10:21994–2002. <https://doi.org/10.1039/C8NR06937A>.
- [32] Jatukaran A, Zhong J, Abedini A, Sherbatian A, Zhao Y, Jin Z, et al. Natural gas vaporization in a nanoscale throat connected model of shale: multi-scale, multi-component and multi-phase. *Lab Chip* 2019;19:272–80. <https://doi.org/10.1039/C8LC01053F>.
- [33] Rigby SP, Gladden LF. The prediction of transport properties of porous media using fractal models and NMR experimental techniques. vol. 54. 1999.
- [34] Rigby SP. A Model for the Surface Diffusion of Molecules on a Heterogeneous Surface 2002. 10.1021/LA0206880.
- [35] Darabi H, Eftehad A, Javadpour F, Sepehrnoori K. Gas flow in ultra-tight shale strata. *J Fluid Mech* 2012;710:641–58. <https://doi.org/10.1017/jfm.2012.424>.
- [36] Holt JK. Fast mass transport through sub-2-nanometer carbon nanotubes. *Science* (80-) 2006;312:1034–7. <https://doi.org/10.1126/science.1126298>.
- [37] Rahmaniyan M, Solano N, Aguilera R. Storage and output flow from shale and tight gas reservoirs. Soc. Pet. Eng. West. North Am. Reg. Meet. 2010 - Collab. with Jt. Meet. Pacific Sect. AAPG Cordillera Sect. GSA, vol. 2, Society of Petroleum Engineers; 2010, p. 1038–58. 10.2118/133611-ms.
- [38] Wang J, Liu H, Zhang H, Luo H, Cao F, Jiao Y, et al. How to correct the petrophysical properties for simulating shale gas production using current commercial simulators? Proc. - SPE Annu. Tech. Conf. Exhib., vol. 2016- January, Society of Petroleum Engineers (SPE); 2016. 10.2118/181321-ms.
- [39] Wu K, Li X, Guo C, Wang C, Chen Z. A unified model for gas transfer in nanopores of shale-gas reservoirs: Coupling pore diffusion and surface diffusion. *SPE J.*, vol. 21, Society of Petroleum Engineers; 2016, p. 1583–611. 10.2118/2014-1921039-PA.
- [40] Hwang S-T, Kammermeyer K. Surface diffusion in microporous media. *Can J Chem Eng* 1966;44:82–9. <https://doi.org/10.1002/cjce.5450440206>.
- [41] Guo L, Peng X, Wu Z. Dynamical characteristics of methane adsorption on monolith nanometer activated carbon. *Huagong Xuebao* 2008;59:2726–32.
- [42] Spanakos D, Rigby SP. Predicting surface diffusivities of gas molecules in shale. *Energy Fuels* 2020;34:12417–28. <https://doi.org/10.1021/acs.energyfuels.0c02441>.
- [43] Cipolla CL, Lolon EP, Erdle JC, Rubin B. Reservoir modeling in shale-gas reservoirs. *SPE Reserv Eval Eng* 2010;13:638–53. <https://doi.org/10.2118/125530-PA>.
- [44] Mengal SA, Wattenbarger RA. Accounting for adsorbed gas in shale gas reservoirs. SPE middle east oil gas show conf. Soc Petrol Eng 2011. <https://doi.org/10.2118/141085-MS>.
- [45] Thompson JM, Okouma Mangha V, Anderson DM. Improved shale gas production forecasting using a simplified analytical method—a marcellus case study. *North Am Unconv Gas Conf Exhib, Soc Petrol Eng* 2011. <https://doi.org/10.2118/144436-MS>.
- [46] Arri LE, Yee D, Morgan WD, Jeanson MW. Modeling coalbed methane production with binary gas sorption. *SPE Rocky Mt Reg Meet, Soc Petrol Eng* 1992. <https://doi.org/10.2118/24363-MS>.
- [47] Hall FE, Chunhe Z, Gasem KAM, Robinson RL, Dan Y. Adsorption of pure methane, nitrogen, and carbon dioxide and their binary mixtures on wet fruitland coal. SPE East Reg Meet, Soc Petrol Eng 1994. <https://doi.org/10.2118/29194-MS>.
- [48] Ambrose RJ, Hartman RC, Diaz-Campos M, Akkutlu IY, Sondergeld CH. Shale gas-in-place calculations Part I: New pore-scale considerations. *SPE J.*, vol. 17, Society of Petroleum Engineers; 2012, p. 219–29. 10.2118/131772-PA.
- [49] Wu K, Li X, Wang C, Yu W, Chen Z. Model for surface diffusion of adsorbed gas in nanopores of shale gas reservoirs. *Ind Eng Chem Res* 2015;54:3225–36. <https://doi.org/10.1021/ie504030v>.
- [50] Huang S, Wu Y, Cheng L, Liu H, Xue Y, Ding G. Apparent permeability model for shale gas reservoirs considering multiple transport mechanisms. *Geofluids* 2018; 2018. <https://doi.org/10.1155/2018/2186194>.
- [51] Wang S, Elsworth D, Liu J. A mechanistic model for permeability evolution in fractured sorbing media. *J Geophys Res Solid Earth* 2012;117. <https://doi.org/10.1029/2011JB008855>.
- [52] Choi J-G, Do DD, Do HD. Surface diffusion of adsorbed molecules in porous media: monolayer. *Multilayer Capillary Condens Regimes* 2001. <https://doi.org/10.1021/ie010195z>.
- [53] Karniadakis G, Beskok A, Aluru N. *Microflows and nanoflows*. Fundam Simulat 2005.
- [54] Kang SM, Fathi E, Ambrose RJ, Akkutlu IY, Sigal RF. Carbon Dioxide Storage Capacity of Organic-Rich Shales n.d.
- [55] Etminan SR, Javadpour F, Maini BB, Chen Z. Measurement of gas storage processes in shale and of the molecular diffusion coefficient in kerogen. *Int J Coal Geol* 2014; 123:10–9. <https://doi.org/10.1016/j.coal.2013.10.007>.
- [56] Cui X, Bustin AMM, Bustin RM. Measurements of gas permeability and diffusivity of tight reservoir rocks: Different approaches and their applications. *Geofluids* 2009;9:208–23. <https://doi.org/10.1111/j.1468-8123.2009.00244.x>.
- [57] Ambrose RJ, Hartman RC, Diaz Campos M, Akkutlu IY, Sondergeld C. New pore-scale considerations for shale gas in place calculations. *SPE Unconv Gas Conf, Soc Petrol Eng* 2010. <https://doi.org/10.2118/131772-MS>.
- [58] Do DD, Do HD. Surface diffusion of hydrocarbons in activated carbon: comparison between constant molar flow, differential permeation and differential adsorption bed methods. *Adsorption* 2001;7:189–209. <https://doi.org/10.1023/A:1012780700536>.
- [59] Do DD, Rice RG. A simple method of determining pore and surface diffusivities in adsorption studies. *Chem Eng Commun* 1991;107:151–61. <https://doi.org/10.1080/00986449108911553>.
- [60] Rigby SP. Predicting surface diffusivities of molecules from equilibrium adsorption isotherms. *Colloids Surfaces A Physicochem Eng Asp* 2005;262:139–49. <https://doi.org/10.1016/j.colsurfa.2005.04.021>.
- [61] Chen YD, Yang RT. Concentration dependence of surface diffusion and zeolitic diffusion. *AIChE J* 1991;37:1579–82. <https://doi.org/10.1002/aic.690371015>.
- [62] Krishna R, van den Broeke LJP. The Maxwell-Stefan description of mass transport across zeolite membranes. *Chem Eng J Biochem Eng J* 1995;57:155–62. [https://doi.org/10.1016/0923-0467\(94\)02951-2](https://doi.org/10.1016/0923-0467(94)02951-2).
- [63] Do HD, Do DD, Prasetyo I. On the surface diffusion of hydrocarbons in microporous activated carbon. *Chem Eng Sci* 2001;56:4351–68. [https://doi.org/10.1016/S0009-2509\(01\)00051-3](https://doi.org/10.1016/S0009-2509(01)00051-3).
- [64] CMG. Computer Modelling Group (CMG). CMOST user guide, Calgary: Computer Modelling Group Ltd. 2019 n.d. <https://www.cmg.ca/> (accessed November 18, 2020).
- [65] Guo C, Wei M, Liu H. Study of gas production from shale reservoirs with multi-stage hydraulic fracturing horizontal well considering multiple transport mechanisms. *PLoS ONE* 2018;13:e0188480. <https://doi.org/10.1371/journal.pone.0188480>.
- [66] Moridis GJ, Blasingame TA, Freeman CM. Analysis of mechanisms of flow in fractured tight-gas and shale-gas reservoirs. *SPE Lat. Am. Caribb. Pet. Eng. Conf. Proc.*, vol. 2, Society of Petroleum Engineers (SPE); 2010, p. 1310–31. 10.2118/139250-ms.
- [67] Ho CK. Dual Porosity vs. Dual Permeability Models of Matrix Diffusion in Fractured Rock. Sandia National Laboratories; 2000.
- [68] Fianu J, Gholinezhad J, Hassan M. Comparison of temperature-dependent gas adsorption models and their application to shale gas reservoirs. *Energy Fuels* 2018; 32:4763–71. <https://doi.org/10.1021/acs.energyfuels.8b00017>.
- [69] Yu W, Sepehrnoori K. Sensitivity study and history matching and economic optimization for marcellus shale. Soc. Pet. Eng. - SPE/AAPG/SEG Unconv. Resour. Technol. Conf., Society of Petroleum Engineers; 2016. <https://doi.org/10.15530/urtec-2014-1923491>.
- [70] Feng X, Ma F, Zhao H, Liu G, Guo J. Gas multiple flow mechanisms and apparent permeability evaluation in shale reservoirs. *Sustainability* 2019;11:2114. <https://doi.org/10.3390/su11072114>.
- [71] Wang HY, Marongiu-Porcù M. A unified model of matrix permeability in shale gas formations. Soc. Pet. Eng. - SPE Reserv. Simul. Symp. 2015, vol. 1, Society of Petroleum Engineers; 2015, p. 103–22. 10.2118/173196-ms.
- [72] Liu F, Ellett K, Xiao Y, Rupp JA. Assessing the feasibility of CO₂ storage in the New Albany Shale (Devonian-Mississippian) with potential enhanced gas recovery using reservoir simulation. *Int J Greenh Gas Control* 2013;17:111–26. <https://doi.org/10.1016/j.ijggc.2013.04.018>.
- [73] vermylen geomechanical studies - Google Search n.d. https://www.google.com/search?q=vermylen+geomechanical+studies&rlz=1C1GCEV_en&oq=vermylen+geomechanical+studies&aqs=chrome..69i57j33.59581j4&sourceid=chrome&ie=UTF-8 (accessed November 18, 2020).
- [74] Strapóč D, Mastalerz M, Schimmelmann A, Drobnik A, Hasenmueller NR. Geochanical constraints on the origin and volume of gas in the New Albany Shale (Devonian–Mississippian), eastern Illinois Basin. *Am Assoc Pet Geol Bull* 2010;94:1713–40. <https://doi.org/10.1306/06301009197>.
- [75] Liu J, Yao Y, Liu D, Cai Y, Cai J. Comparison of pore fractal characteristics between marine and continental shales. *Fractals* 2018;26:1840016. <https://doi.org/10.1142/S0218348X18400169>.
- [76] Pei P, Ling K, He J, Liu Z. Shale gas reservoir treatment by a CO₂-based technology. *J Nat Gas Sci Eng* 2015;26:1595–606. <https://doi.org/10.1016/J.JNGSE.2015.03.026>.
- [77] Hosseini E, Gholami R, Hajivand F. Geostatistical modeling and spatial distribution analysis of porosity and permeability in the Shurijeh-B reservoir of Khangiran gas field in Iran. *J Pet Explor Prod Technol* 2019;9:1051–73. <https://doi.org/10.1007/s13202-018-0587-4>.